AALBORG UNIVERSITET

Brain Insulin Resistance in the Experimental (TgSwDI) Mouse Model of Alzheimer's Disease

Kathrine Overgaard Jensen

Medicine with Industrial Specialization

Biomedicine

2025

AALBORG UNIVERSITET

Title:

Brain Insulin Resistance in the Experimental (TgSwDI) Mouse Model of Alzheimer's Disease

Semester:

10th semester

Project period:

September 1st, 2024 - May 28th, 2025

ECTS:

60 points

Project group:

9026

Supervisor:

Torben Moos

Participants:

Kathrine Overgaard Jensen (20193684)

Total pages: 78

Normal pages: 53

Appendix: 13 pages

TABLE OF CONTENTS

Abbreviations

Aβ: Amyloid beta

AD: Alzheimer's Disease

Akt: Protein Kinase B

BBB: Blood-brain barrier

BECs: brain endothelial cells

BIR: Brain insulin resistance

CNS: Central nervous system

CREB: cAMP response element-binding protein

CSF: Cerebrospinal fluid

ECD: The extracellular domain

GLUT: Glucose transporter

Grb-2: Growth factor receptor-bound protein 2

GSK-3: Glycogen synthase kinase-3

HKP: Housekeeping protein

HybRs: Hybrid receptors

IDE: Insulin-degrading enzyme

IGF: Insulin-like growth factor

IGF-1R: Insulin-like growth factor 1 receptor

IGFBPs: Insulin-like growth factor binding proteins

IL: interleukin

ILC: Internal loading control

INSR: Insulin receptor

IP: Intraperitoneal

IRS: Insulin receptor substrate

JM: Juxtamembrane

L1,L2: Leucine-rich repeat domains 1,2

MAPK: Mitogen-activated protein kinase

mTOR: mammalian target of rapamycin

PI3K: Phosphoinositide 3-kinase

PIP2: Phosphatidylinositol 4,5-biphosphate

PIP3: Phosphatidylinositol (3,4,5)-trisphosphate

PTEN: phosphatase and tensin homolog

pY: Phospho-Y

ROS: Reactive oxygen species

SHC: Src homology and collagen

T2DM: Type 2 diabetes mellitus

TK: Tyrosine kinase

TMD: Transmembrane domain

UDP-GlcNAc: Uridine 5'-diphosphate-N-acetylglucosamine

WB: Western blot

WT: Wild-type

Abstract

Aim: This project aims to evaluate the underlying mechanisms of brain insulin resistance (BIR) in Alzheimer's disease (AD) by investigating the insulin receptor (INSR) and insulin-like growth factor 1 receptor (IGF-1R) signaling pathways in an experimental (TgSwDI) mouse model of AD. Detection of expression and phosphorylation levels of INSR and IGF-1R was conducted. A higher INSRα-A/B ratio at the level of the blood-brain barrier (BBB) has recently been associated with BIR in AD brains. The objective of this project is to replicate these findings and validate the potential of using the INSRα-A/B ratio as a marker of BIR in future research.

Methods: With a particular focus on the BBB, three samples from each mouse were obtained, including total brain and isolated capillary and brain fractions. The brain capillary depletion technique was used to separate brain capillaries from brain fractions. This technique was validated using cresyl violet staining. Western blot (WB) analyses were performed to detect the protein content of INSRα isoforms and IGF-1R in TgSwDI mice aged 18 and 30 months and wild-type (WT) mice aged 12 months. Phosphorylation levels of INSR and IGF-1R were further analyzed using WB analyses following intraperitoneal (IP) injections of either insulin or saline in TgSwDI mice aged 15 months and WT mice aged 12 months.

Results: INSRα-A and INSRα-B were primarily concentrated in isolated capillary fractions rather than total brain and brain fractions. This project did not demonstrate a higher INSRα-A/B ratio in isolated capillary fractions, serving as a potential marker of BIR. Due to low protein concentrations in the brain fractions, the protein content of IGF-1R in isolated capillary fractions compared to capillary-depleted brain fractions could not be determined. Increased protein content of IGF-1R in TgSwDI mice compared to WT mice was demonstrated. No significant differences in phosphorylation levels of INSR and IGF-1R were observed between TgSwDI and WT mice.

Conclusion: In conclusion, this project highlights new insights into BIR by investigating INSR and IGF-1R signaling in an experimental (TgSwDI) mouse model of AD. Conflicting data exists regarding the roles of INSR and IGF-1R signaling in AD patients and the experimental model examined here, which necessitates more comparative research.

1. Introduction

1.1 Alzheimer's Disease

Alzheimer's disease (AD) is an incurable, neurodegenerative disorder characterized by a progressive decline or loss in memory and cognition [1]. After the age of 65, the prevalence of AD doubles every 5 years [2]. AD contributes to 60-70% of all dementia cases, and it is estimated that dementia impacts more than 55 million individuals worldwide [1], [3]. Each year this number is expected to enhance by 10 million new cases [1], [3]. Approximately 97.000 individuals at the age of 65 or older are living with dementia in Denmark [4]. This number is predicted to exceed 145.000 by 2040 [4]. The increased prevalence of AD is driven by a growing elderly population and longer life expectancies [5]. Early stages of AD are usually initiated with short-term memory loss and changes in attention and problem-solving abilities [6]. As AD advances, the disease pattern is commonly defined by personality changes, language impairments and loss of insight [6]. In the latest stages of AD, individuals are entirely dependent on healthcare workers for all daily activities [6].

To date, no effective treatment strategies for slowing down the progression of AD have been revealed [1]. An incomplete understanding of AD's underlying cause is associated with the failure of new drug candidates in clinical trials [1]. The amyloid cascade hypothesis has been the most well-known hypothesis for years, proposing that amyloid beta (Aβ) and hyperphosphorylated tau are the primary causes [1]. However, the amyloid cascade hypothesis has been criticized and questioned in recent years [1], [5]. Clinical trials have not confirmed the efficacy of drugs capable of eliminating these proteins [1], [5]. In addition, Aβ plaques are absent in an increased number of AD patients, further weakening the amyloid cascade hypothesis [1]. These findings have led researchers to explore other possible causes of AD. One suggested hypothesis is that AD is a metabolic disease characterized by a disrupted ability to use glucose for energy due to insulin resistance [1], [7]. Evidence indicates that brain glucose metabolism may begin to decrease more than 10 years before dementia symptoms appear [1]. This suggests a potential association between brain metabolic changes and AD development [1].

1.2 Definition of Brain Insulin Resistance

Insulin resistance has been linked to type 2 diabetes mellitus (T2DM) for many years [8], [9], [10] and the definition has expanded over time [8]. Today, insulin resistance is defined as a reduced biological response to insulin that impacts glucose metabolism and various reactions to insulin, such as cell growth, differentiation and protein synthesis [8]. Insulin resistance has been identified in insulin-sensitive tissues, such as the liver, adipose tissue and muscle [11]. Currently, there is growing evidence that insulin resistance can likewise occur in the brain and develop independently of diabetes [8], [9], [12], [13]. This phenomenon is referred to as brain insulin resistance (BIR) [1]. BIR can be defined as the impaired ability of brain cells to effectively respond to circulating insulin [1], [14], [15]. The reduced response of brain cells to insulin may stem from several mechanisms, such as downregulated insulin receptor (INSR) expression, ineffective insulin binding or disruptions in the insulin signaling pathway [9], [15], [16]. Along with disruptions in the insulin signaling pathway, abnormalities in the insulin-like growth factor (IGF) signaling pathway have been linked to BIR [17], [18], [19], [12]. BIR is characterized by declined insulin transport across the blood-brain barrier (BBB) and a decreased presence of insulin in the brain [1], [10], [20]. Overall, BIR can manifest as dysfunctions in metabolic regulation and impairments in mood and cognition [8], [9], [14]. Over 25 years ago, Hoyer introduced the concept of BIR in AD as a possible factor of the glucose hypometabolism identified in AD [21], [22]. Since then, extensive research has shown reduced levels of insulin, INSRs, IGF-1 receptors (IGF-1Rs), insulin receptor substrates (IRSs) and decreased phosphorylation of Protein Kinase B (Akt) and glycogen synthase kinase-3 (GSK-3) in AD brains [9], [18], [23], [24]. The most substantial evidence comes from human postmortem studies identifying signs of insulin resistance in the brain of AD patients with disruptions in signal transduction [7], [12]. Declined expression levels of INSR and IGF-1R have been demonstrated to begin early and progress with the disease [7], [24]. These findings further support the concept that disruptions in the insulin and IGF signaling pathways play a key role in the pathogenesis of AD [7], [24]. To date, the term type 3 diabetes is often considered to explain the hypothesis that BIR may contribute to the development of AD [14], [18]. The term highlights AD as a brain-specific form of diabetes, sharing features with type 1 and T2DM [14], [18].

1.3 Contributors to Brain Insulin Resistance

1.3.1. Insulin

1.3.1.1 The Role of Insulin in the Brain

The primary function of insulin is to regulate body energy metabolism, with glucose metabolism being its main target [1], [7]. Glucose is the brain's primary energy source [1], [7], and the brain uses around 25% of the body's glucose while at rest [1]. In contrast to peripheral tissues, insulin in the brain only plays a minimal role in regulating the cellular uptake of glucose [12], [13]. Brain uptake and utilization of glucose are mediated by specific glucose transporter (GLUT) proteins [1]. The primary transporters in the brain, GLUT-1 and GLUT-3, function independently of insulin [1], [7], [20]. The transport of glucose into glial cells and brain endothelial cells (BECs) relies primarily on GLUT-1, while the most common transporter in neurons is GLUT-3 [25]. Evidence suggests that the insulin-dependent GLUT-4 is identified in a few selected nuclei [25] in specific areas of the brain, including the hippocampus, olfactory bulb, cerebellum and neocortex [1], [20], [25]. GLUT-4 has been shown to help transport glucose into synapses during periods of high synaptic activity [1]. Additionally, the expression of GLUT-4 in the brain is much less common than GLUT-1 and GLUT-3, suggesting that the brain does not store glucose in response to insulin [1], [26]. Consequently, the brain has been considered an insulin-insensitive organ for many years [19], [25]. Today, the brain is regarded as a key target for insulin action, with INSRs initiating intracellular signaling pathways essential for maintaining proper brain functions [1], [19]. Evidence suggests that insulin is crucial for the regulation of fundamental processes in the brain, such as nutrient homeostasis, reproduction, cognition, food intake, body weight, brain perfusion and regulation of mood [10], [11], [25], [26]. Administration of insulin to animals has been reported to increase expression levels of INSR in the hippocampus [26], [27] and improve memory and learning processes [25], [28]. Insulin maintains several neuroprotective roles in the brain, such as neuronal survival and enhancing synaptic plasticity [11]. It is postulated that insulin can protect cells from Aβ-induced cell death by inhibiting the formation of Aβ fibrils [25]. Furthermore, the activity of insulin-degrading enzyme (IDE) increases in the presence of insulin [1], [10]. Lower levels of IDE are often a key feature of BIR, which may result in increased deposition of Aβ plaques in the brain [1], [10]. Insulin exerts

neuromodulatory effects by regulating the density of neurotransmitter receptors, suppressing norepinephrine and stimulating serotonin reuptake in neuronal cells [11], [25]. By targeting vascular BECs, insulin can control capillary constriction and relaxation [1]. This mechanism helps maintain the integrity of the BBB and the removal of Aβ from brain tissue to the blood vessels [1]. As a result, BIR may lead to elevated BBB permeability, disrupted blood pressure regulation and increased levels of Aβ in the brain [1].

1.3.1.2 How does Insulin get to the Brain?

Previously, insulin was viewed as a peripheral hormone unable to pass through the BBB and influenced the central nervous system (CNS) [29]. The ability of insulin to pass through the BBB was first noticed by Margolis and Altszuler [30]. They found that peripheral insulin administration led to elevated insulin levels in rats' cerebrospinal fluid (CSF) [30]. Similar results were examined in dogs [25], [31]. Although insulin administration caused a rapid increase in blood insulin levels, only a modest rise in insulin levels within the CSF was detected [25], [31]. These observations indicated a non-linear relationship between insulin levels in plasma and CSF, suggesting that insulin might cross the BBB mediated by a saturable transport system [25], [32]. Today, it is generally accepted that insulin primarily passes the BBB through BECs via INSR-mediated transcytosis [14], [33]. Insulin can cross the BBB into brain regions, such as the hypothalamus, pons-medulla, striatum, hippocampus, frontal cortex and parietal cortex [34]. In specific brain areas, including the arcuate nucleus of the hypothalamus, the BBB is found to be less dense [35]. Multiple factors, such as inflammation, diabetes mellitus, high-fat diet and triglyceride levels, appear to influence the permeability of the BBB [9], [14]. Whether insulin in the brain is produced locally or originates primarily from the pancreatic islet cells is still an ongoing debate [19], [32]. C-peptide, a byproduct of insulin synthesis, has been observed in the CSF [14], [25]. Post-mortem studies of human brain tissues have identified insulin mRNA, particularly in brain areas such as the hippocampus and hypothalamus [9], [24]. The presence of insulin mRNA has also been confirmed in specific brain regions of rats and mice [36], [37]. Research revealed insulin production in cultured neurons from rats, which was secreted when their membranes were depolarized by potassium and calcium ions [29], [38]. This insulin production in neurons may occur in pyramidal neurons in specific brain areas, such

as the hippocampus, olfactory bulb and prefrontal cortex [29], [39] and does not seem to occur in glial cells [29]. Moreover, less than 1% of insulin crosses the BBB in dogs and rodents, further supporting the idea that insulin production occurs within the brain itself [29]. Although data demonstrates that brain cells can produce insulin, the phenomenon has not yet been confirmed. Instead, it is generally believed that most insulin in the brain originates from the pancreatic cells [19].

1.3.2 Brain Insulin Receptors

Usually, peripheral insulin resistance can be clinically measured on fasting insulin and glucose levels using the homeostatic model assessment for insulin resistance (HOMA-IR) [13]. By contrast, the definition of BIR remains less clarified [13]. As previously described, brain INSRs are not directly involved in the classic glucose-insulin feedback mechanism, and blood insulin levels can remain unaffected by disrupted insulin activity in the brain [1], [13]. Additionally, since the brain does not act as a glucose reservoir, BIR may not necessarily result in reduced glucose levels in the brain [10]. As a result, assessing BIR can be challenging, and to date, no well-established method for measuring BIR exists [1], [13]. Therefore, BIR is often considered and measured as a disruption in the insulin signaling pathway [10], [13].

1.3.2.1 Location and Structure

The olfactory bulb is reported to have the highest expression levels of INSR in the brain [40], [41]. In addition, INSRs have been identified in other brain areas, including the hippocampus, cerebral cortex, cerebellum, striatum and hypothalamus [9], [40]. Further research has found the presence of INSRs in nearly all cell types in the brain, especially in neurons in presynaptic terminals and dendrites [40], [41]. This distribution highlights their involvement in synapse formation and dendritic growth [41]. By examining the brain's vasculature, INSRs are especially enriched in capillaries [42]. Structurally, the INSR is organized as a dimer of heterodimers, referred to as $(\alpha\beta)_2$ [43]. The INSR comprises two extracellular α-chains and two transmembrane β-chains (Fig. 1) [43]. The extracellular domain (ECD) includes the α-chain and the first 190 residues of the β-chain at the N-terminus [43]. The ECD is composed of two

leucine-rich repeats (L1 and L2), a cysteine-rich region (CR) and the fibronectin type III domains, FnIII-1, FnIII-2 and FnIII-3 [43], [44]. The FnIII-2 domain includes an insert domain (ID-α), composed of the α/β furin cleavage site [44], [45]. The α-CT is a peptide segment from the C-terminal region of the ID-α component [44], [45]. Depending on the exclusion and inclusion of exon 11, the length of the α-CT segment differs between INSRα-A and INSRα-B [45]. In the absence of ligands, the ECD forms a symmetrical λ-shaped structure [45], [46]. This structure includes the L1-CR-L2 module of one monomer and the FnIII-1, FnIII-2 and FnIII-3 modules of the opposing monomer [45], [46]. The remaining β-subunit passes through the cell membrane by a transmembrane domain (TMD) [44], [45], [46]. The TMD consists of intracellular domains, such as the juxtamembrane (JM), tyrosine kinases (TKs) and the C-terminal (CT) domain [44], [45], [46]. Intermonomer disulfide bonds are observed in the FnIII-1 domains and the ID-α components [45], [46]. Moreover, a disulfide bond in each monomer connects ID-α to the FnIII-3 domain located within the β-chain [45], [46].

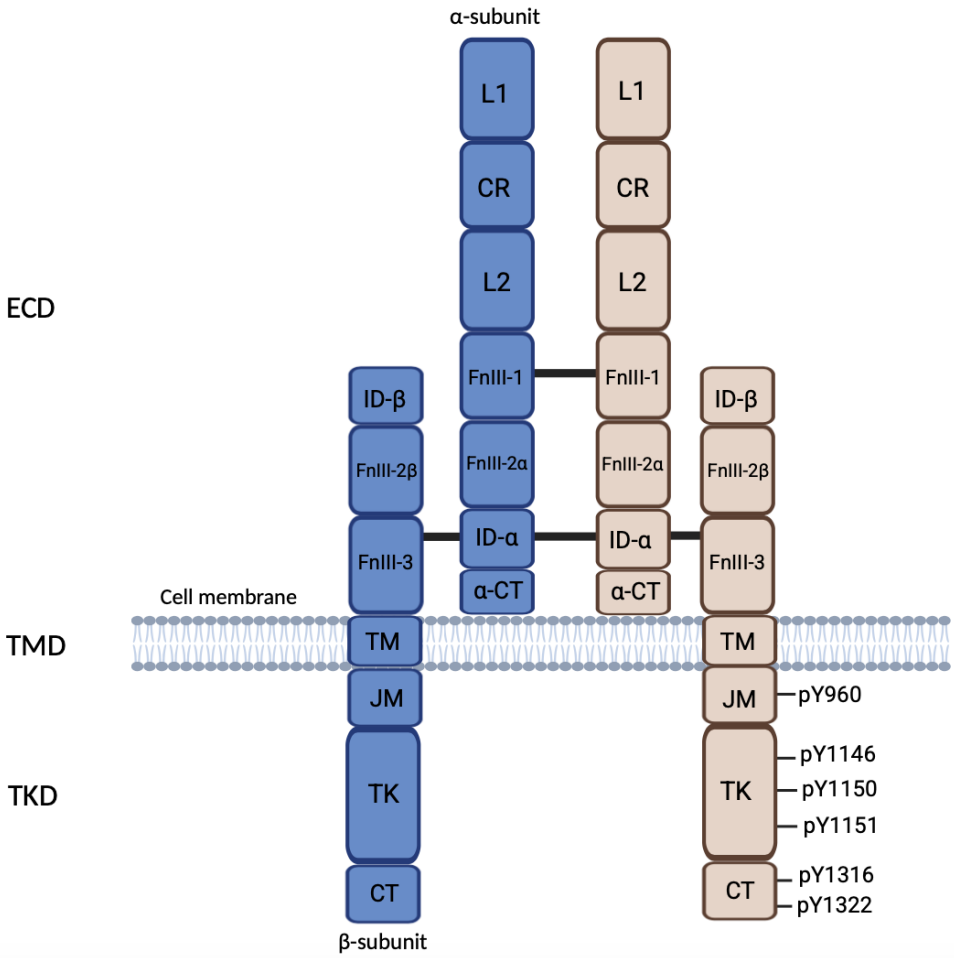

Fig. 1. Illustration of the insulin receptor composed of two α-subunits and two β-subunits. Disulfide bonds are shown as black lines. L1, L2: leucine-rich repeat domains 1,2, CR: cysteine-rich region, FnIII-1, 2, 3: fibronectin type III domains 1, 2, 3, ID-α: insert domain α, α-CT: α C-terminal domain, TM: transmembrane, JM: juxtamembrane, TK: tyrosine kinase, CT: C-terminal, ECD: extracellular domain, TMD: transmembrane domain, TKD: tyrosine kinase domain, pY: phospho-Y. Created in Biorender. Figure inspired by Yunn et al. (2023) [47] and Scapin et al. (2018) [43].

The β-subunits of the INSR undergo dimerization upon insulin binding to the α-subunits, which induces a conformational change of the INSR [9], [44]. These mechanisms lead to the activation of TKs and autophosphorylation of the β-subunits [9], [44]. Multiple tyrosine residues in the intracellular region of the INSR undergo phosphorylation [44]. This includes phospho-Y1316 (pY1316) and pY1322 in the CT domain, pY1146, pY1150 and pY1151 within the activation loop of the TK domain along with pY960 in the JM domain (Fig. 1) [44]. Phosphorylation of tyrosine residues creates binding sites for adaptor proteins, IRS-1/2 and Src homology and collagen (SHC) [44]. This process leads to the activation of different downstream signaling cascades, including the phosphoinositide 3-kinase (PI3K)/Akt and Ras-mitogen-activated protein kinase (MAPK) pathways (Fig. 2) [44].

1.3.2.2 PI3K/Akt Signaling Pathway

Upon binding of IRS-1 and IRS-2 to the INSR, phosphorylation of several tyrosine residues on IRS occurs. [9], [44]. This process creates binding sites for the regulatory p85 subunit of PI3K (Fig. 2) [29], [41]. In addition, PI3K becomes activated and translocates to the plasma membrane [29], [41]. The catalytic p110 subunit of PI3K converts phosphatidylinositol 4,5-biphosphate (PIP2) to phosphatidylinositol (3,4,5)-trisphosphate (PIP3). This leads to the recruitment of the serine (Ser)/threonine (Thr) kinase Akt to the plasma membrane [29], [41], [48]. PIP3 activates 3-phosphoinositide-dependent protein kinase-1 (PDK1), which further phosphorylates Akt at its Thr308 site at the plasma membrane [41], [48], [49]. However, complete Akt activation requires phosphorylation at the Ser473 site by the mammalian target of rapamycin complex 2 (mTORC2) [41], [48], [49]. Activated Akt leads to stimulation of different

downstream targets such as inhibitor of nuclear factor kappa-B kinase (IKK), mouse double minute 2 homolog (MDM2) and cAMP response element-binding protein (CREB) [9], [49]. These proteins control various mechanisms, including cytokine production, transcription and cell survival [9], [49]. Moreover, Akt inhibits proteins that play a key role in regulating apoptosis, including bcl-2-associated death promoter (BAD), caspase 9 (CASP9) and forkhead box O (FOXO) protein and thereby supporting cell survival (Fig. 2) [9], [49]. The PI3K-Akt pathway is controlled by certain negative regulators, such as the phosphatase and tensin homolog (PTEN), protein phosphatase 2 (PP2A) and PH-domain leucine-rich-repeat-containing protein phosphatases (PHLPP1/2) [49]. PTEN functions by suppressing Akt signaling through the conversion of PIP3 to PIP2 [49]. Similarly, PP2A and PHLPP1/2 suppress Akt signaling by dephosphorylating Thr308 or Ser473 sites on Akt [49].

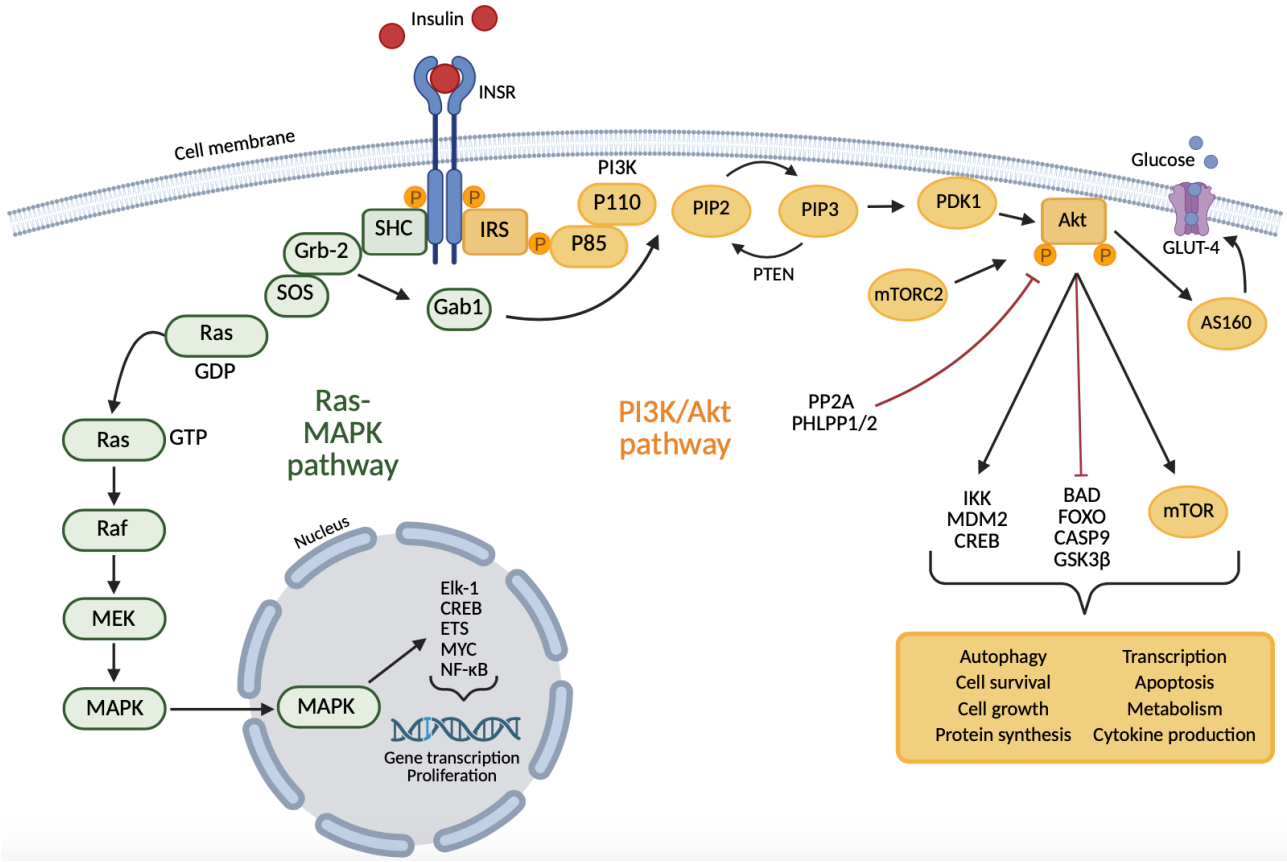

Fig. 2. Overview of the PI3K/Akt and Ras-MAPK signaling pathways. Insulin receptor activation leads to phosphorylation of tyrosine residues on insulin receptor substrates 1/2. This process activates the PI3K complex, leading to further activation of Akt. Activated Akt initiates several downstream effects, such as

activation of mTOR, translocation of GLUT-4 to the plasma membrane and inhibition of GSK-3β. These mechanisms regulate critical cellular functions such as growth, survival and autophagy. The Ras-MAPK signaling pathway is initiated when SHC proteins bind to the insulin receptor, which triggers a downstream phosphorylation cascade involving Ras, Raf, MEK and MAPK. Activated MAPK enters the nucleus to regulate gene expression, cell differentiation, proliferation and survival. Akt: Protein Kinase B, BAD: bcl-2-associated death promoter, FOXO: forkhead box O, Grb-2: growth factor receptor-bound protein 2, GSK-3β: glycogen synthase kinase 3β, MAPK: mitogen-activated protein kinase, MEK: mitogen-activated protein kinase kinase, MDM2: mouse double minute 2 homolog, mTOR: mammalian target of rapamycin, mTORC2: mammalian target of rapamycin complex 2, PDK1: 3-phosphoinositide-dependent protein kinase-1, PI3K: phosphoinositide 3-kinase, PTEN: phosphatase and tensin homolog, Raf: rapidly accelerated fibrosarcoma, SHC: Src homology and collagen, Gab1: Grb2-associated binder-1, SOS: son of sevenless, Ras: Rat sarcoma virus oncogene, Elk-1: Ets-like protein, CREB: cAMP response element-binding protein, INSR: insulin receptor, NF-κB: Nuclear factor-κB, PP2A: protein phosphatase 2, PHLPP1/2: PH-domain leucine-rich-repeat-containing protein phosphatases, PIP2: phosphatidylinositol 4,5-biphosphate, PIP3: phosphatidylinositol (3,4,5)-trisphosphate, AS160: Akt substrate of 160 kDa. Created in Biorender. Figure inspired by Arnold et al. (2018) [9], Leiphrakpam et al. (2024) [50] and Gabbouj et al. (2019) [41].

Alterations in the PI3K-Akt pathway in AD patients primarily manifest as reduced phosphorylation or overall levels of components within the signaling cascade [41]. BIR is characterized by increased levels of proinflammatory cytokines, such as tumor necrosis factor α (TNFα), C-reactive protein (CRP), monocyte chemotactic protein-1 (MCP-1) and interleukins (ILs) [1]. TNFα impairs the activity of IRS-1 and suppresses GLUT-4 expression, whereas IL-1 lowers IRS-1 expression [1]. Moreover, IL-6 may promote IRS degradation [1]. As previously described, insulin does not participate directly in the regulation of glucose metabolism in the brain. However, growing evidence suggests that insulin may regulate it through non-traditional pathways to some extent [19]. Firstly, Akt is responsible for the regulation of glucose uptake in certain neurons by phosphorylation of Akt substrate of 160 kDa (AS160), which translocates GLUT-4 to the cell membrane (Fig. 2) [9], [41]. Therefore, disruptions in the PI3K-Akt signaling pathway may lead to reduced GLUT-4 activity [1]. Secondly, decreased glucose uptake in the brain has been demonstrated in FDG-PET imaging of astrocyte-specific INSR knock-out mice

[27]. The reduction was associated with lower GLUT-1 expression in the brain [27]. Thirdly, it is believed that insulin may indirectly promote the translocation of GLUT-3 to the plasma membrane in neurons [19]. Due to the brain's minimal ability to store glucose, a reduced supply can quickly impair its function [1]. Disrupted brain glucose metabolism can impair mitochondrial aerobic respiration and thereby lead to damage of the mitochondria [51]. Mitochondrial damage is observed early in the AD brain and plays an essential role in the development of oxidative stress, leading to elevated reactive oxygen species (ROS) production [51]. Overproduction of ROS increases Aβ accumulation and causes oxidative damage to nucleic acids, proteins and lipids [1], [52]. Research indicates that ROS may influence energy metabolism in the brain by regulating the permeability of neuronal cells to glucose [52]. Decreased energy metabolism in the brain can potentially increase the activity of BACE1 and thereby lead to further Aβ formation [1]. In addition, a reduction in the number of GLUTs reduces uridine 5'-diphosphate-N-acetylglucosamine (UDP-GlcNAc) levels [1]. Normally, UDP-GlcNAc functions by binding to tau and APP by O-GlcNAc transferase, leading to O-GlcNAcylation, which inhibits their phosphorylation [1]. Therefore, lower UDP-GlcNAc levels can contribute to tau and APP hyperphosphorylation and consequently lead to neurotoxicity [1].

The mammalian target of rapamycin (mTOR) is activated by the PI3K-Akt pathway [9]. mTOR is responsible for the regulation of different processes such as protein synthesis, transcription, cell growth, division, survival and autophagy (Fig. 2) [9], [44], [51]. Insufficient glucose utilization in the brain may decrease the ability to clear misfolded proteins through autophagy, which consequently can promote Aβ accumulation [1]. Beclin 1 is considered a key protein that initiates autophagy, and the levels of Beclin 1 have been found to decline in AD brains [1]. Furthermore, GSK-3β serves as another target protein for Akt [29]. Under normal conditions, the PI3K-Akt pathway results in the phosphorylation of GSK-3β at its Ser9, which promotes GSK-3β inactivation [29]. In AD, this inhibition is impaired, contributing to GSK-3β activation. GSK-3β is a key mediator of tau hyperphosphorylation, further leading to the construction of neurofibrillary tangles [16], [41]. Overall, activation of GSK-3β is associated with neuronal death and damage, elevated production and accumulation of Aβ, memory and learning

deficits, cytoskeletal instability, promotion of pro-inflammatory responses and apoptosis [16], [51], [53],[54]. Insulin has been demonstrated to reduce tau phosphorylation by inhibiting GSK-3β via PI3K-Akt signaling in cultured neurons [41]. This highlights the potential of using GSK-3β regulation as a strategy to prevent damaging processes in AD.

1.3.2.3 Ras-MAPK Signaling Pathway

Recruitment of either the Grb-2-SOS complex or SHC adaptor proteins can initiate activation of the Ras-MAPK pathway [48], [55]. SHC proteins bind to the phosphorylated tyrosine residues on the INSR via its SH2 or phosphotyrosine binding (PTB) domain [55]. This results in tyrosine phosphorylation of its calponin homology 1 domain (CH1), resulting in the recruitment of the SH2 domain of Grb-2 (Fig. 2) [55]. Besides SH2 domains, Grb-2 contains SH3 domains which interface with SOS proteins, leading to activation of Ras by replacement of GDP with GTP [29], [48]. The activation of Ras recruits the Ser/Thr kinase Raf, which further leads to the activation of mitogen-activated protein kinase kinase (MEK/MAPK) [29], [55]. Finally, MEK phosphorylates and activates MAPK [29], [55]. Overall, this process leads to the translocation of phosphorylated MAPK into the nucleus and regulates various transcription factors [55]. Transcription factors involved in this process are Elk-1, CREB, ETS, MYC and NF-κB [29], [55]. They are responsible for the regulation of gene expression, cell differentiation, proliferation, survival, apoptosis and neuroplasticity [9], [29], [55]. Grb-2 connects the PI3K-Akt and Ras-MAPK signaling pathways due to the binding of Grb-2's SH3 domain to Grb2-associated binder-1 (Gab1) (Fig. 2) [55]. Once bound, Gab1 undergoes tyrosine phosphorylation and activates the PI3K-Akt signaling pathway [55]. While INSR signaling promotes the Ras-MAPK signaling pathway, it appears to be more active in response to IGF-1R signaling [55].

1.3.3 INSRα Isoforms

The INSR α-chain is presented in two isoforms, identified as INSRα-A and INSRα-B. INSRα-A and INSRα-B differ by 12 amino acids caused by alternative splicing of exon 11 [10], [44], [56]. Therefore, exon 11 is present in INSRα-B (Fig. 3A) [10], [44], [56]. The INSRα isoforms are

especially found to differ in terms of function and tissue distribution [45]. Research suggests that INSRα-A mainly supports cell survival, growth and proliferation [57]. Furthermore, tissue distribution of INSRα-A includes the brain, fetal tissue, ovaries, testes and the spleen [45], [46]. High expression levels of INSRα-B have been observed in adult differentiated cells [10], [17]. This isoform is especially distributed in tissues important for insulin metabolism and regulation of metabolic processes [10], [17]. This includes the liver, kidney, adipose tissue and skeletal muscle [10], [45], [48], [58]. INSRα-A is mainly believed to trigger the Ras-MAPK signaling pathway, while INSRα-B activates the PI3K/Akt signaling pathway [19]. Moreover, the distribution of INSRα isoforms in the brain varies across different cell types. INSRα-A is mainly expressed by neurons, while INSRα-B is primarily observed in BECs, microglia and astrocytes (Fig. 3B) [9], [10], [46]. Variations in transcription and maturation processes are believed to contribute to the abundance of INSRα isoforms [10]. INSRα-A and INSRα-B have been studied in different metabolic diseases, such as obesity and diabetes and in various peripheral organs, including the liver, muscle and adipose tissue [56]. Current data suggests that a higher INSRα-A/B ratio has been identified in the liver of individuals with T2DM [10], [56], while a similar elevation has been observed in adipocytes of obese individuals [56]. After diabetes remission and weight loss, the INSRα-A/B ratio in these individuals returned to normal [56]. These data suggested that an increase in the INSRα-A/B ratio may disrupt the insulin signaling pathway and contribute to insulin resistance [10], [46]. Therefore, an elevated INSRα-A/B ratio may be used as a molecular index of insulin resistance [46], [56]. An altered INSRα-A/B ratio has recently been linked to BIR [56]. A study by Calon et al. investigated the expression levels of INSRα isoforms at the level of the BBB by using post-mortem human brains and a 3xTg mouse model [56]. Calon and coworkers reported that INSRs, particularly INSRα-B, were enriched in microvessels in contrast to microvessel-depleted parenchymal fractions [56]. In addition, AD brains showed reduced levels of INSRα-B in microvessels compared to control brains. No vascular difference of INSRα-A was detected between AD and control brains, resulting in a higher vascular INSRα-A/B ratio [56]. Furthermore, vascular INSRα levels demonstrated an inverse correlation with Aβ plaques and a positive correlation with Aβ degradation factors such as IDE [56]. This study by Calon et al. is the first to demonstrate BIR at the level of the BBB by identifying an altered INSRα-A/B ratio [56]. Overall, data from this study highlights that changes

in INSRα isoforms at the level of the BBB may impact brain insulin signaling, which potentially could offer new insights into therapeutic targets for AD [10], [42], [56].

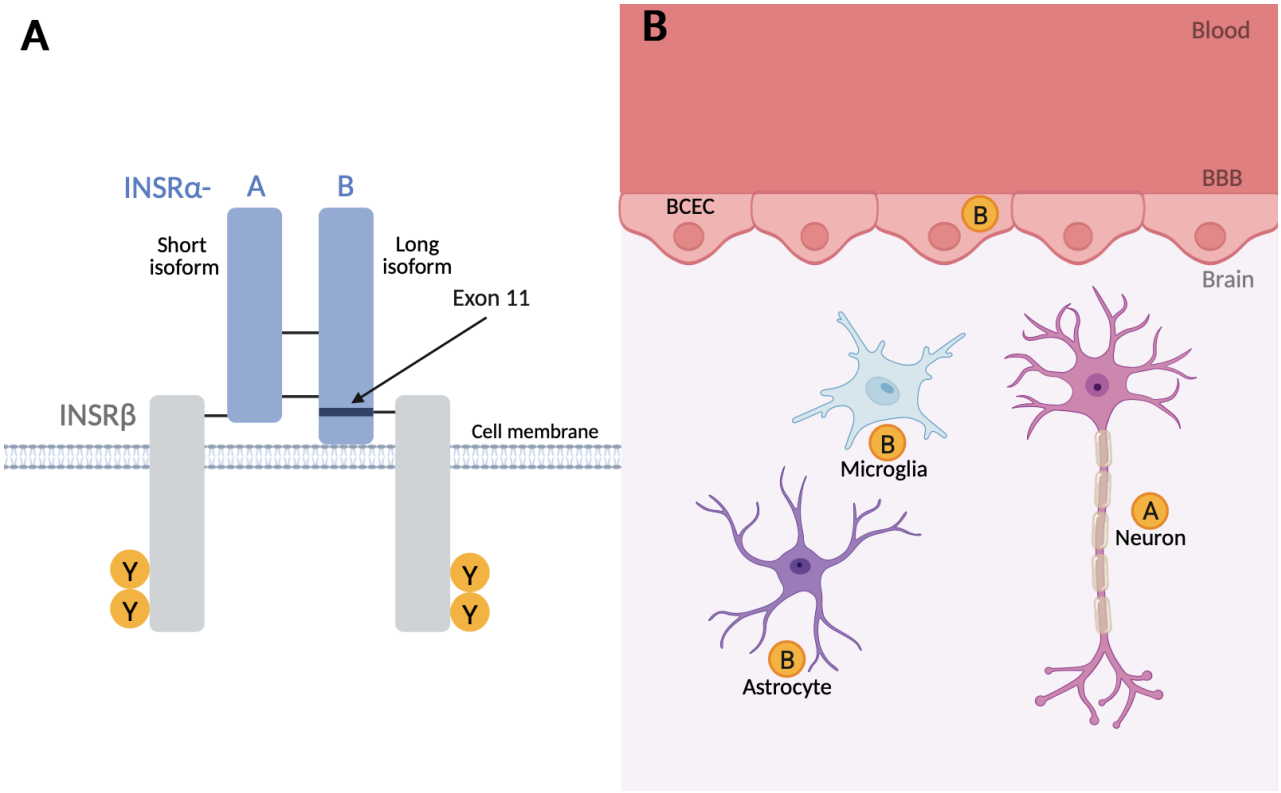

Fig 3. (A) Illustration of INSRα-A and INSRα-B. INSR has two splice variants, the short A isoform (INSRα-A) and the long B isoform (INSRα-B). INSRα isoforms differ by the inclusion of exon 11 in INSRα-B, encoding a 12 amino acid region. (B) Distribution of INSRα isoforms in different brain cells. INSRα-A is primarily found in neurons, while brain endothelial cells, microglia and astrocytes mainly express INSRα-B. INSR: Insulin receptor, BBB: Blood-brain barrier, BCEC: Brain capillary endothelial cell. Created in Biorender. Figure inspired by Rhea et al. (2024) [10].

In addition to their function and tissue distribution, INSRα isoforms are believed to differ in ligand binding affinities [45]. INSRα-A exhibits a slightly higher binding affinity for insulin compared to INSRα-B (Fig. 4) [45], [46], [48]. However, INSRα-A and INSRα-B vary extensively in their binding affinities for the IGF ligands IGF-1 and IGF-2 [45], [48]. INSRα-A generally exerts a higher affinity for IGF-1 and IGF-2, particularly for IGF-2, compared to INSRα-B (Fig. 4) [44], [45], [48], [57]. Recent data indicate that the functions of INSRα isoforms are primarily

influenced by their binding affinities for IGF-1 and IGF-2 rather than by their slightly different binding affinities for insulin [46].

1.3.3.1 IGF-signaling

The IGF system consists of the IGF-1R and IGF-2 receptor (IGF-2R), the growth factors IGF-1 and IGF-2 and a group of six insulin-like growth factor binding proteins (IGFBPs) [59], [60]. The INSR and IGF-1R share about 70% sequence similarity [61] and include the same structural domains [62]. Ligand binding initiates phosphorylation of three tyrosine residues within the TK domain, pY1131, pY1135 and pY1136 [48], resulting in activation of the PI3K/Akt and Ras/MAPK signaling pathways [17], [58]. IGF-1 and IGF-2 serve as activators of IGF-1R [63], although IGF-1R is believed to have the highest affinity for IGF-1 (Fig. 4) [48], [60]. Insulin can bind to IGF-1Rs, and similarly, IGFs can bind to INSRs, but both interactions have lower affinity than their primary ligands [60]. However, INSRα-A binds IGF-2 with an affinity comparable to that of insulin (Fig. 4) [63], [64]. The IGF-2R lacks tyrosine activity and serves as a decoy receptor. Therefore, the binding of IGF-2 to IGF-2R will inhibit IGF-2-dependent signaling through INSRα-A and IGF-1R [45], [65]. Most IGFs are bound to IGFBPs, which may affect the overall signaling potential of IGF ligands [17], [60], [65]. IGFBPs regulate the availability of IGF-1 and IGF-2 by restricting the interaction between IGF ligands and their receptors, leading to reduced signaling activity of IGFs [65].

Usually, plasma IGF-1 peaks in puberty and progressively declines with age [17]. Lower levels of IGF-1 are observed to be reached by the age of 75 [66], [67]. Although the expression levels of IGF-1R are markedly reduced in adult brains, the levels remain relatively high in brain areas such as the choroid plexus, meninges and vascular sheaths [17]. IGF-1 maintains several vital effects in the CNS, such as inhibition of apoptosis and regulation of both adult and embryonic neurogenesis. Moreover, IGF-1 supports cell survival, maturation and the differentiation of nerve cells within the CNS [17], [59], [68], [69]. IGF-1R is widely distributed in BECs of the intact brain and isolated brain microvessels in humans and mice [70]. IGF-1R has been observed in the rodent CNS in neuronal precursor cells, with particularly elevated levels during certain developing phases, such as olfactory bulb formation and midbrain development [17]. A high

distribution of IGF-1Rs has been observed in the hippocampus and amygdala in human postmortem studies [17]. Overall, conflicting data exist concerning the expression levels of IGF-1R in AD brains. Multiple studies have observed increased IGF-1R levels in AD brains [23], [71], [72], [73], [74], whereas other studies showed the opposite [24], [74].

1.3.3.2 Hybrid receptors

In specific cells, co-expression of the INSRα isoforms can occur. Co-expression of both isoforms can lead to the formation of two homodimers, INSRα-A or INSRα-B [19], [45], and heterodimer formation, resulting in INSRα-A/INSRα-B hybrid receptors (HybRs) (Fig. 4) [45]. Similarly, INSR and IGF-1R can form heterodimeric HybRs, which results from the high degree of structural similarity and shared signaling pathways between INSR and IGF-1R [17], [58]. INSRα isoforms can form heterodimers with IGF-1R by combining the α- and β-subunits of the INSR with the α- and β-subunits of the IGF-1R [45], [75]. The presence of two INSRα isoforms leads to the formation of either INSRα-A/IGF-1R or INSRα-B/IGF-1R (Fig. 4) [45], [46]. It is generally accepted that INSR/IGF-1R HybRs consist of two ligand-binding sites. One binding site is presented in the L1 domain of the INSR and the α-CT segment of the IGF-1R [45], [46]. The location of the other ligand binding site is in the L1 domain of the IGF-1R and the α-CT segment of the INSR [45], [46]. The formation of HybRs can occur in all tissues and cell types expressing both receptors [76], [77]. As a result, HybRs have been found to have higher expression levels than INSR and IGF-1R homoreceptors [46]. Evidence suggests that INSR/IGF-1R HybRs can bind both IGF-1, IGF-2 and insulin [19], [44]. However, INSR/IGF-1R HybRs are believed to mainly support IGF signaling [19], [63], and recent data demonstrate that they show a much greater affinity for IGF-1 compared to insulin (Fig. 4) [46], [48], [78]. Therefore, current data highlights a potential link between the formation of HybRs and insulin resistance, as these receptors exert a low affinity for insulin [61], [76], [79]. Overall, it remains unclear whether HybRs have distinct signaling properties compared to homodimers, and determination of the exact function of HybRs in the brain requires further investigations [44], [46], [76].

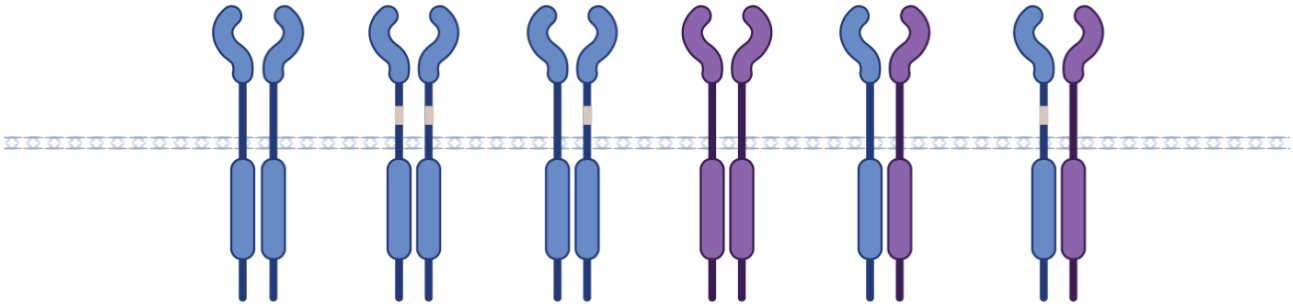

	INSRα-A	INSRα-B	INSRα-A/ INSRα-B	IGF-1R	INSRα-A/ IGF-1R	INSRα-B/ IGF-1R
Insulin	++++	+++	++++	+	++	+
IGF-1	+++	+	++	++++	++++	++++
IGF-2	++++	++	+	+++	++++	++

Fig. 4. An overview of the insulin and insulin-like growth factor signaling pathways. The receptors can form homodimers or heterodimers. Each receptor binds insulin, IGF-1 or IGF-2 with varying degrees of affinity. Ligand affinities are reported as follows: + (very low), ++ (low), +++ (high) and ++++ (very high). IGF-2R serves as a decoy receptor and is not presented in this figure. References to the various ligand binding affinities are mentioned in the body text. INSR: Insulin receptor, IGF-1R: Insulin-like growth factor 1 receptor, IGF-1: Insulin-like growth factor 1, IGF-2: Insulin-like growth factor 2. Created in Biorender. Illustration inspired by Escribano et al. (2017) [48] and Lee et al. (2022) [65].

1.4 Aim of Study

Assessing BIR can be challenging, and the phenomenon is often measured as a disruption in the insulin signaling pathway. The recent study by Calon et al. was the first to demonstrate a higher INSRα-A/B ratio in AD at the level of the BBB [56], serving as a potential marker of BIR. The results indicate that changes in the INSRα isoforms at the level of the BBB may contribute to the development of BIR. To date, no conclusive evidence exists supporting this finding. Along with disruptions in the insulin signaling pathway, abnormalities in the IGF signaling pathway have been linked to BIR. However, the association between AD and IGF-1R expression levels is characterized by conflicting data. Therefore, this study aims to examine whether BIR at the level of the BBB can be demonstrated in an experimental (TgSwDI) mouse model of AD with a particular focus on:

1. Investigations of the INSRα isoforms (INSRα-A and INSRα-B), especially the INSRα-A/B ratio.
2. Assessment of IGF-1R expression levels.
3. Examination of phosphorylation levels of INSR and IGF-1R following insulin injections.

2. Materials and Methods

2.1. Western Blotting

2.1.1 Animals

All animal experiments followed relevant guidelines and regulations (EU Directive 2010/63/EU) (License no.: 2024-15-0201-01691). This project included TgSwDI mice *(n = 19)* and C57BL/6J wild-type (WT) mice *(n = 10)* (Fig. 5). To investigate the expression levels of INSRα isoforms and IGF-1R, TgSwDI mice aged 18 months *(n = 6 males)* and 30 months *(n = 2 females and 3 males)* were used. These findings were compared to data from 12-month-old WT mice *(n = 4 females)* (Fig. 5). To further investigate the phosphorylation levels of INSR and IGF-1R, insulin injections in 15-month-old TgSwDI mice *(n = 4 males)* were performed along with saline injections in TgSwDI mice of the same age *(n = 4 males)*. In addition, 12-month-old WT mice were exposed to insulin injections *(n = 3 females)* and saline injections *(n = 3 females)* (Fig. 5).

The TgSwDI mouse model is a widely studied model of AD based on the genetic background of the C57BL/6 WT mouse [80]. TgSwDI mice express the human amyloid precursor protein (APP) gene under the control of the mouse Thy1 promoter [80], [81]. The APP gene consists of the Swedish (K670N/M671L), Dutch (E693Q) and Iowa (D694N) mutations [80]. Currently, an association between mutations in the APP gene and the development of cerebral amyloid angiopathy has been found [82]. The Dutch and Iowa APP mutations lead to the accumulation of Aβ40, whereas the Swedish APP mutation produces Aβ40/42 peptides [80], [81]. The TgSwDI mouse model is characterized by rapid and excessive Aβ accumulation, particularly in cerebral microvessels [81], [82]. Therefore, this model serves as a useful tool for studying the BBB and its changes following Aβ deposition. Research suggests that Aβ accumulation in TgSwDI mice begins at age 2-3 months with widespread deposits by 12 months [80], [81], [83]. Increased amounts of Aβ plaques have been detected in the hippocampus and neocortex in TgSwDI mice at 12-15 months old [80]. Furthermore, these findings have been confirmed in mice aged 15 months in the thalamus [80].

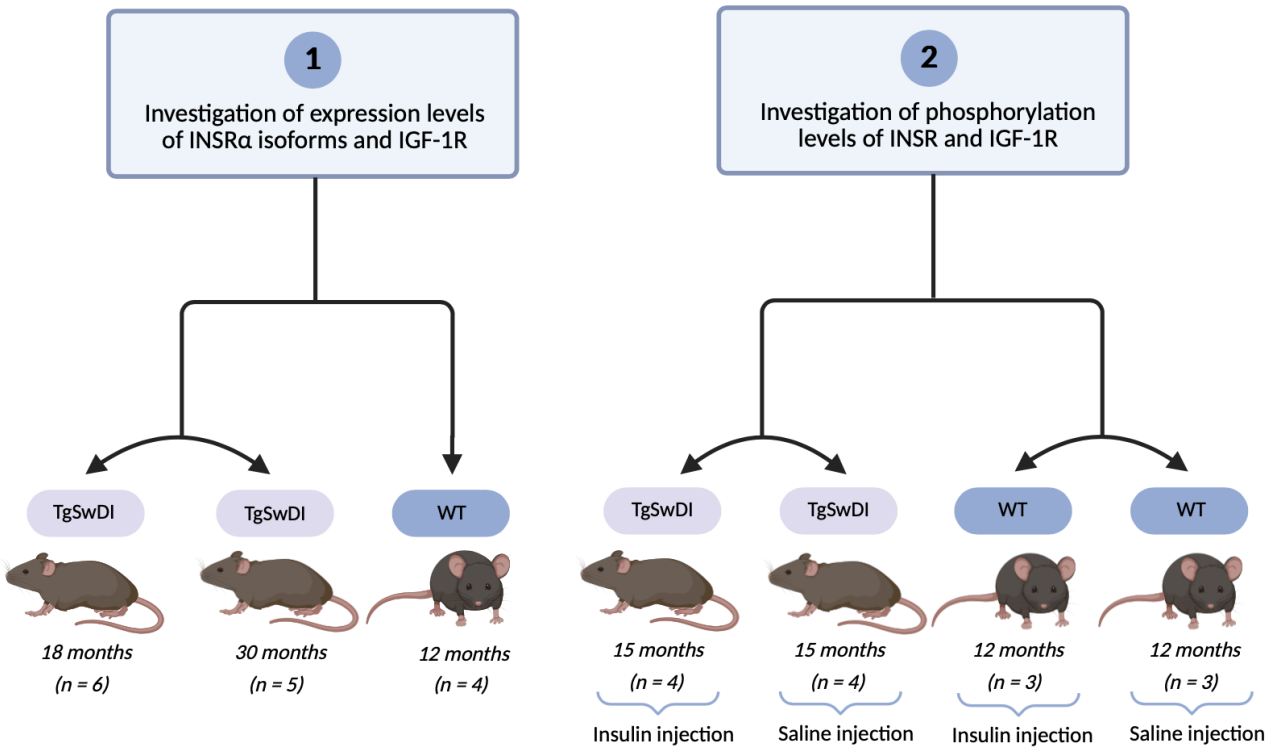

Fig. 5: Overview of TgSwDI mice (n = 19) and wild-type (WT) mice (n = 10) used in this project. TgSwDI mice aged 18 months (n = 6) and 30 months (n = 5) were used to investigate INSRα isoforms and IGF-1R expression levels. The results were compared to data from WT mice aged 12 months (n = 4). Insulin and saline injections were conducted in 15-month-old TgSwDI mice (n = 8) and 12-month-old WT mice (n = 6) to investigate the phosphorylation levels of INSR and IGF-1R. Created in Biorender.

2.1.2 Brain Capillary Depletion Technique

The following experimental procedures were performed to obtain three samples from each mouse, including total brain, fraction obtained by isolating brain capillaries and the remaining brain fraction (Fig. 6). The experimental procedures outlined below were initiated by assessing the blood glucose levels of each mouse following 2 hours of fasting.

2.1.2.1. Investigation of Expression Levels of INSRα Isoforms and IGF-1R

The mice were deeply anesthetized, and transcardial perfusion was conducted using Potassium Phosphate Buffered Saline (KPBS). Following the isolation of the brains, the

prefrontal cortex was sectioned off and frozen. The prefrontal cortex was later utilized as the total brain sample for western blot (WB) (Fig. 6). The procedure was followed by the brain capillary depletion technique in accordance with a previous study [84]. The remaining brains were homogenized in 525 μl ice-cold capillary depletion buffer (10 mM Hepes, 141 mM NaCl, 4 mM KCl, 2,8 mM $CaCl_2$, 1 mM $MgSO_4$, 1 mM NaH_2PO_4 and 10 mM glucose; pH 7,4) and 2 mL of ice-cold 30% dextran (MW 60,000, Sigma-Aldrich). The dextran-containing solutions were centrifuged at 5400 x g for 40 minutes at 4°C in a Fresco 21 microcentrifuge (Thermo Fisher Scientific). After centrifugation, two fractions were obtained, including the capillary-depleted supernatant and the capillary-enriched pellet. The supernatant, including the brain "cake" was separated from the pellet. Further WB analyses were conducted using the supernatants as the brain fraction samples and the pellets as the capillary samples (Fig. 6). All samples were frozen at -70°C.

2.1.2.2. Investigation of Phosphorylation Levels of INSR and IGF-1R

The examination of phosphorylation levels of INSR and IGF-1R was performed using a procedure closely resembling the procedure described above, with minor modifications (Fig. 6). An intraperitoneal (IP) injection of either 0,15 mL saline or Insulatard FlexPen (Novo Nordisk A/S), containing 100 IE/ml of human insulin, was applied. 30 minutes after IP injection, each mouse was anesthetized. Following the similar procedure reported above, three samples from each mouse were collected and frozen at -70°C. IP injections of saline served as controls.

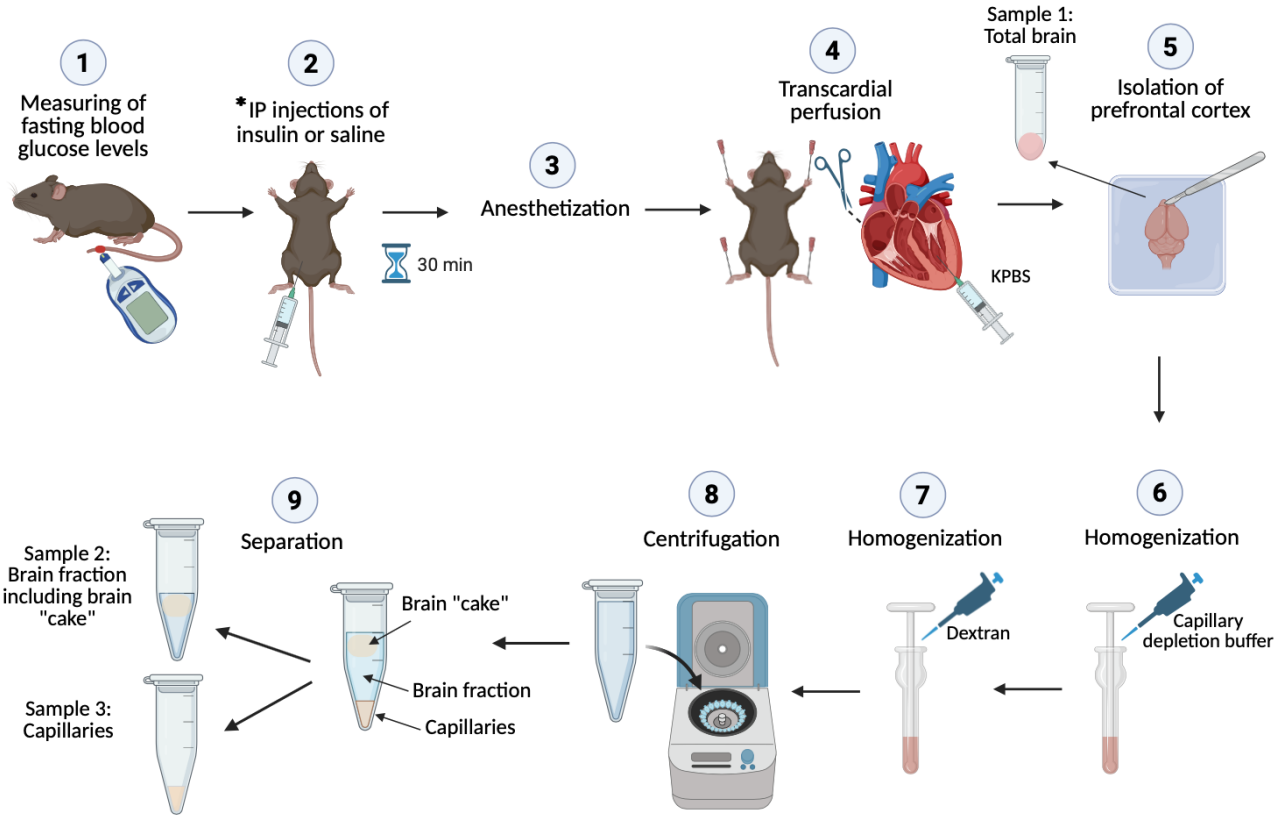

*Fig. 6: Illustration of the experimental procedures performed to obtain three samples from each mouse, including total brain, fraction obtained by isolating brain capillaries and the remaining brain fraction. Fasting blood glucose levels of each mouse were measured following 2 hours of fasting. The mice were anesthetized and exposed to transcardial perfusion. The prefrontal cortex was isolated and transferred to a separate Eppendorf tube (sample 1). Two homogenization steps of the remaining brains were conducted using capillary depletion buffer and dextran. Centrifugation of the samples resulted in a capillary-depleted supernatant, including the brain "cake", which was separated (sample 2) from the capillary-enriched pellet (sample 3). The procedure described was used to investigate the expression levels of INSRα and IGF-1R. *The phosphorylation levels of INSR and IGF-1R were investigated following a similar procedure with a slight modification. Intraperitoneal injections of either insulin or saline were applied before the anesthetization of the mice. Created in Biorender.*

2.1.3. Sample Preparation for Western blotting

The total brain samples were lysed in Neuronal Protein Extraction Reagent (N-PER) (87792, Thermo Fisher Scientific) containing cOmplete™ Mini EDTA-free protease inhibitor cocktail

(Sigma-Aldrich) by using a homogenizer. N-PER was added at a ratio of 10 mL per 1 g of tissue. The fractions obtained by isolating brain capillaries were homogenized following the same procedure but using 200 μl of N-PER. All homogenates were incubated on ice for 10 min. After incubation, the samples were centrifuged at 10.000 x g for 10 minutes at 4°C. The supernatants were collected. Preparation of the capillary-depleted brain fraction samples included two centrifugation steps for 40 minutes followed by 20 minutes at 10.000 x g and 4°C. This procedure made it possible to separate and discard the brain "cake" from the remaining sample. The Pierce™ BCA Protein Assay Kit (23225, Thermo Fisher Scientific) was used to determine the total protein concentration in each sample according to the manufacturer's procedure.

2.1.4. Western Blotting Procedure

Revert™ 700 Total Protein Stain (LI-COR) was used for WB normalization. To analyze the expression levels of INSRα isoforms, 25 μg of protein was loaded on the gels. In contrast, a loading concentration of 50 μg was used to assess the expression levels of IGF-1R and phosphorylation levels of the receptors. The samples were mixed with 1X NuPAGE LDS Sample Buffer (NP0007, Thermo Fisher Scientific) and 1X NuPAGE Sample Reducing Agent (NP0009, Thermo Fisher Scientific). The samples were heated for 10 minutes at 70℃ followed by loading on NuPAGE™ 4-12% Bis-Tris gels (NP0323, Thermo Fisher Scientific). 5 μL PageRuler™ Plus Prestained Protein Ladder (26619, Thermo Fisher Scientific) was added to all gels. Each sample was separated by gel electrophoresis at 120V for 2 hours using 1X NuPage MES SDS Running buffer (NP0002, Thermo Fisher Scientific). The separated proteins were electroblotted onto nitrocellulose membranes (LC2001, Thermo Fisher Scientific) at 30V for 1 hour using 1X NuPage Transfer buffer (NP0006-1, Thermo Fisher Scientific) and 10% methanol (Sigma-Aldrich). After transfer, the nitrocellulose membranes were fully dried for 10 minutes in an oven at 37℃. The membranes were incubated in 1X Phosphate Buffered Saline (PBS) for 5 minutes at room temperature. Prior to staining, the membranes were rinsed in ultrapure water. Staining of the membranes was conducted by incubation in Revert™ 700 Total Protein Stain solution (LI-COR) for 5 minutes. The membranes were rinsed twice in Revert™ Wash Solution (LI-COR) for

30 seconds, followed by a washing step with ultrapure water. The total protein stain image was acquired using the Odyssey Fc Imager with Image Studio 5.0 (LI-COR). Nonspecific binding was blocked by 1-hour incubation of the nitrocellulose membranes in blocking buffer. 1X PBS containing 3% Tween 20 (Sigma-Aldrich) was used to block the membranes for further analysis of INSRα isoforms. Membranes for analyzing IGF-1R and phosphorylation levels were blocked in 1X PBS containing 3% skim milk powder and 2% Tween 20 (Sigma-Aldrich). The membranes were incubated at 4℃ overnight with primary antibodies diluted in washing buffer consisting of 1X PBS and 0,05% Tween 20 (Sigma-Aldrich). As used in the previous study by Calon et al. [56], this project aimed to examine the INSRα isoforms by using the human insulin R/CD220 primary antibody (1:500, AF1544, R&D Systems) [85]. Primary antibodies used to investigate the IGF-1R and phosphorylation levels were IGF-1Rα (2C8) (1:200, sc-463 HRP, Santa Cruz Biotechnology) [86] and Phospho-IGF-I Receptor β (Tyr1131)/Insulin Receptor β (Tyr1146) (1:1000, 3021, Cell Signaling Technology) [87]. The membranes were rinsed in washing buffer and incubated with secondary antibodies diluted in washing buffer for 1 hour at room temperature. Secondary antibodies used in this project were HRP-conjugated anti-goat IgG (1:10.000, 705-035-147, Jackson ImmunoReseach) [88] for INSRα isoforms, similar to Calon et al. [56] and HRP-conjugated anti-rabbit IgG (1:5.000, sc-2004, Santa Cruz Biotechnology) [89] for detection of the phosphorylation levels. The Pierce™ ECL Western Blotting Substrate (32109, Thermo Fisher Scientific) was used to visualize protein blots. WB bands were acquired using the Odyssey Fc Imager with Image Studio 5.0 (LI-COR). Normalized signal values of the target proteins and total protein stain were calculated using Empiria Studio Software 3.2 (LI-COR).

2.1.5. Statistical tests

Data were analyzed using GraphPad Prism 10.2. The threshold for statistically significant data was $P < 0.05$. The Shapiro-Wilk normality tests were performed on all data. If two groups were compared and the data was not normally distributed, a paired test was performed using the Wilcoxon matched-pairs signed rank test, while the Mann-Whitney U test was applied if the data was unpaired. When unpaired data from three groups were normally distributed, parametric one-way ANOVA was used, followed by Tukey's multiple comparisons test. However, if variances were different, the Welch-ANOVA followed by Dunnett's multiple

comparisons test was applied. Normally distributed paired data from three groups were analyzed using the repeated one-way ANOVA, followed by Tukey's multiple comparisons test. In contrast, the Friedmann test was conducted if the data was not normally distributed. Comparisons of four unpaired groups were detected using the Kruskal-Wallis test, followed by Dunn's multiple comparisons test in the presence of data that was not normally distributed.

2.1.6 Cresyl violet staining

Cresyl violet staining was performed to validate the brain capillary depletion technique. 3 μl of each sample was transferred to coverslips. The samples were fixated for 20 minutes at 60℃. Filtrated 0,4% cresyl violet solution (cresyl violet acetate, Milli-Q water, 1 M NaAcetate, 1 M acetic acid) was used to stain the samples for 5 minutes at room temperature. The coverslips were rinsed in ultrapure water for 2 minutes and mounted with Pertex.

3. Results

3.1 Brain Capillary Depletion Technique Validation

The brain capillary depletion technique used to separate brain capillaries was validated using cresyl violet staining. The enrichment of vascular structures in the isolated capillary fractions demonstrated that the brain capillary depletion technique was reliable (Fig. 7).

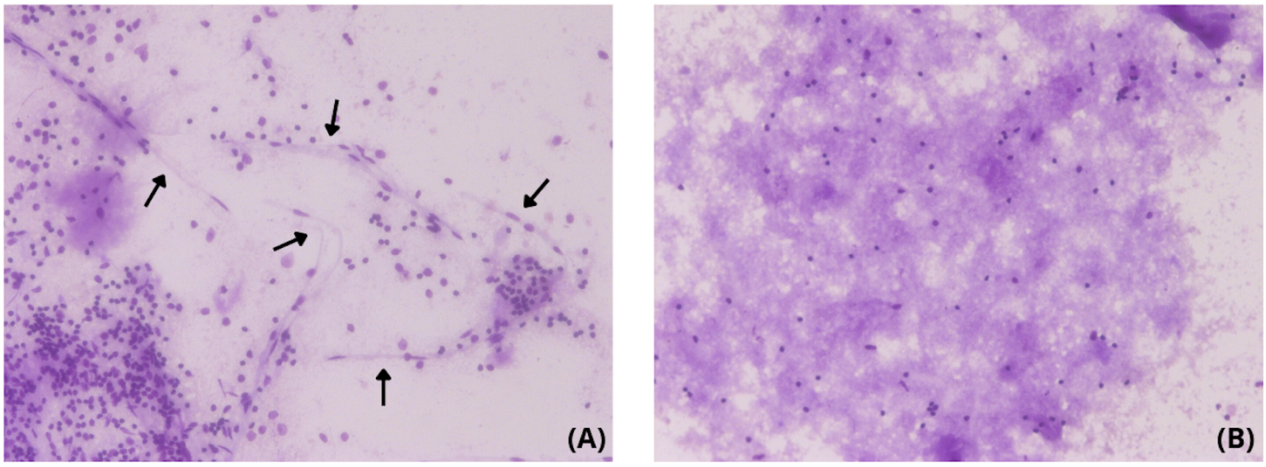

Fig. 7. Cresyl violet staining to validate the brain capillary depletion technique (20x). (A) Isolated capillary fraction enriched in vascular structures (black arrows). (B) Brain fraction sample with unidentifiable vascular structures. Cellular nuclei are seen as small dark dots.

3.2 Fasting Blood Glucose Levels

To evaluate the diabetic status of TgSwDI and WT mice, fasting blood glucose levels of each mouse were measured (Fig. 8). As reported in previous studies [90], [91], a fasting blood glucose level exceeding 200 mg/dL, was considered diabetic. For each TgSwDI and WT mouse, only a single mouse exceeded the diabetic threshold of 200 mg/dL, indicating that most of the mice used in this project were non-diabetic.

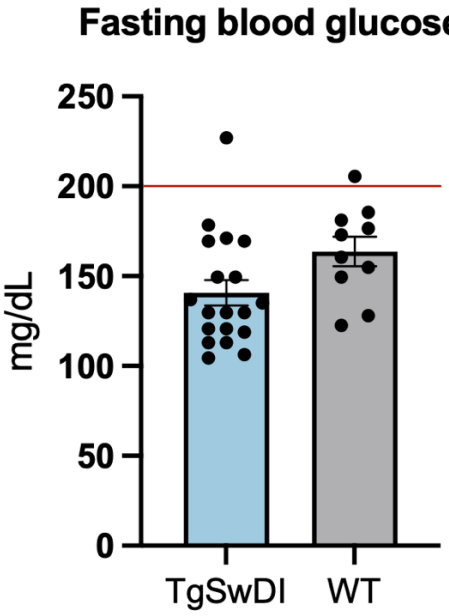

Fig. 8. Concentrations of fasting blood glucose levels of TgSwDI (n = 19) and wild-type (n = 10) mice. The diabetic threshold of 200 mg/dL is depicted as a red line. The fasting blood glucose levels are below the diabetic threshold in all but two measurements. Exceptions are observed in TgSwDI and wild-type mice, where one mouse in each group exceeds 200 mg/dL. Data is depicted as mean ± SEM. WT: Wild-type.

3.3 Protein Content of INSRα Isoforms

In accordance with the previous study of Calon et al. [56], this project aims to determine the expression levels of INSRα isoforms in the mouse brain. The analyses involved three samples from each mouse, including total brain and isolated capillary and brain fractions. WB analyses of INSRα isoforms revealed two separated bands at ~130 kDa [56], identified as INSRα-A and INSRα-B (Fig. 9A). An overview of the WB bands detecting INSRα isoforms can be found in Appendix A.1. To identify the most suitable WB protein concentration, various concentrations were tested (Fig. 9B). 25 μg protein was concluded to be the optimal loading concentration, as this concentration allowed differentiation between the INSRα isoforms (Fig. 9B). To ensure that the target protein and total protein stain both display a linear relationship between sample loading and band intensity, a linear range of detection was conducted. The linear range of detection was performed by blotting several protein concentrations on a membrane (15-45 μg) (Fig. 9C). The membrane was stained with total protein stain (Fig. 9D), and a linear range of

detection was separately determined for the target protein and total protein stain (Fig. 9E). These ranges were combined to observe a level of sample loading that would produce a linear response for both. The green segments reflect the optimal range of protein to load. Loading of 25 μg protein does not fall within green segments for both the target protein and total protein stain. However, it still illustrates good linearity (Fig. 9E).

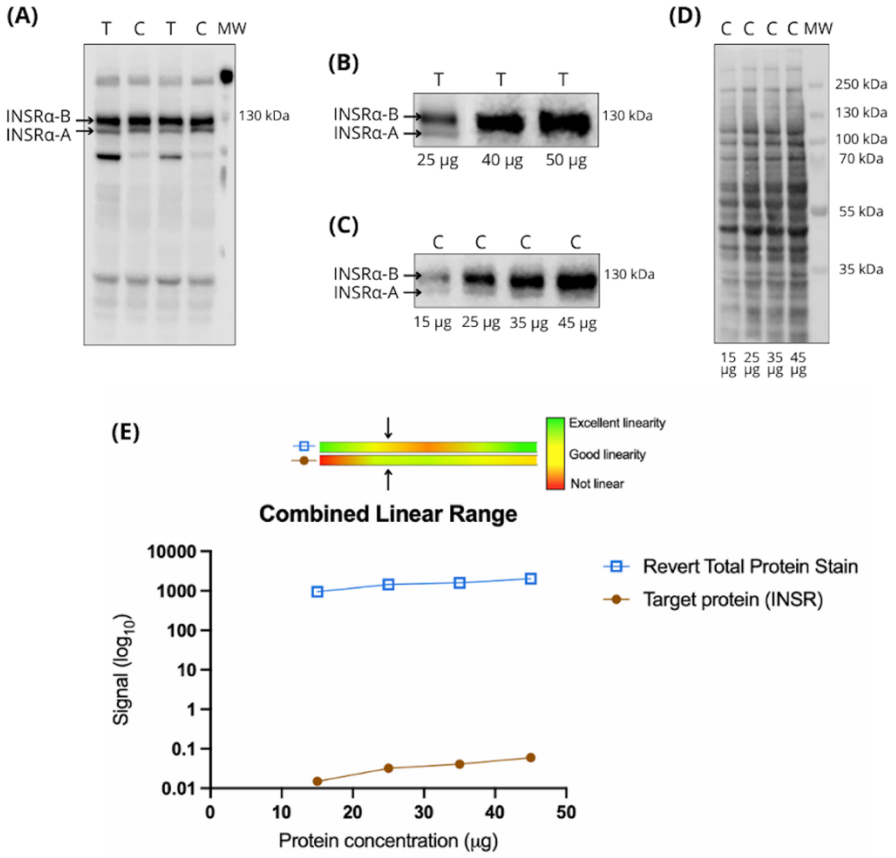

Fig. 9. (A) Illustration of a blotting membrane obtained by Western blot analysis of the expression levels of INSRα isoforms. The INSRα isoforms are identified as two separated bands at ~130 kDa [56]. An overview of the remaining WB bands detecting INSRα isoforms is shown in Appendix A.1. (B) Three different protein concentrations (25 µg, 40 µg, and 50 µg) were used to determine the optimal Western blot loading concentration. Based on the result, 25 µg was the optimal loading concentration, allowing differentiation between the INSRα isoforms. (C) Various protein concentrations of the target protein (15 µg, 25 µg, 35 µg, and 45 µg) were used to assess the linear range of detection. (D) The membrane was stained with total protein stain to visualize and evaluate actual sample loading across the blot. (E) The target protein and total protein stain were analyzed within the combined linear range. With 25 µg of protein loaded, the combined linear range of the target protein and total protein stain represented good

linearity. The combined linear range was calculated using Empiria Studio Software 3.2 (LI-COR). Data are plotted on a logarithmic 10 scale. T: Total brain, C: Capillaries, MW: Molecular weight, INSR: Insulin receptor.

This project found that in both TgSwDI and WT mice, INSRα-A and INSRα-B were concentrated in total brain and isolated capillary and brain fractions (Fig. 10). Visualization of the WB bands indicated slightly increased signal intensities of INSRα-B in the isolated capillary fractions compared to total brain (Fig. 10A and Appendix A.1). Additionally, the signal intensities of the brain fraction samples were observed to be markedly reduced compared to the remaining samples. To investigate if the visual differences between each mouse were significant, comparative tests were conducted. The normalized signal values of INSRα-A in total brain and isolated capillary and brain fractions were compared in TgSwDI and WT mice (Fig. 10B and C). For TgSwDI mice (Fig. 10B), the repeated one-way ANOVA found significant differences between the samples ($p < 0.05$). The Tukey's multiple comparisons test was applied for further analysis, showing significant differences between total brain and isolated capillary and brain fractions (Fig. 10B and Table 1). Data from WT mice (Fig. 10C) were analyzed using the Friedman test. Significant differences were detected ($p < 0.05$), and Dunn's multiple comparisons test found a significant difference between isolated capillary and brain fractions ($p = 0.0140$). The remaining groups were considered non-significant ($p > 0.05$) (Fig. 10C).

Table 1. Tukey's multiple comparisons test performed on INSRα-A in TgSwDI mice with corresponding p-values.

INSRα-A	**P-value**
Total brain (TgSwDI) vs. capillaries (TgSwDI)	0.0023
Total brain (TgSwDI) vs. brain fraction (TgSwDI)	0.0036
Capillaries (TgSwDI) vs. brain fraction (TgSwDI)	0.0023

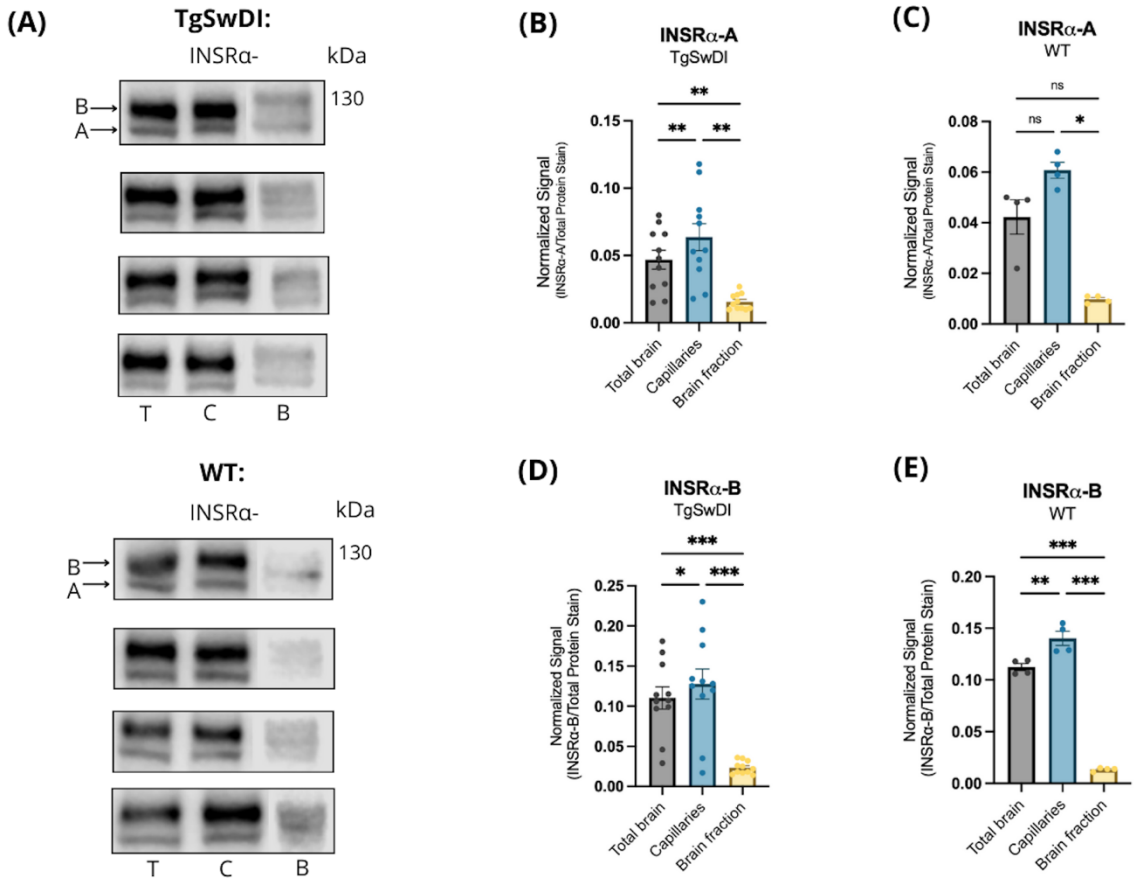

*Fig. 10. (A) Representative Western blots of TgSwDI and wild-type mice show enriched content in INSRα isoforms, particularly INSRα-B, in total brain and isolated capillary fractions. The presence of INSRα isoforms in brain fraction samples was reduced compared to total brain and isolated capillary fractions. (B-E) Scattered bar plots of normalized signal values for INSRα-A and INSRα-B in TgSwDI and wild-type mice between total brain and isolated capillary and brain fractions. Data depicted as mean ± SEM and analyzed with repeated one-way ANOVA followed by Tukey's multiple comparisons test, n = 11 (B and D), n = 4 (E) or Friedman test followed by Dunn's multiple comparisons test, n = 4 (C). *p <0.05, **p <0.01, ***p <0.001. T: Total brain, C: Capillaries, B: Brain fraction, INSR: Insulin receptor, WT: Wild-type, Non-significant.*

Similarly to INSRα-A, normalized signal values of INSRα-B in total brain and isolated capillary and brain fractions were compared in TgSwDI and WT mice (Fig. 10D and E). Tukey's multiple comparisons tests found significant differences between total brain and isolated capillary and

brain fractions for TgSwDI and WT mice (Fig. 10D-E and Table 2). In conclusion, significant differences of INSRα-A were observed between total brain and isolated capillary and brain fractions in TgSwDI mice. A similar observation was identified in WT mice between isolated capillary and brain fractions. Significant differences of INSRα-B in total brain and isolated capillary and brain fractions were further determined for both TgSwDI and WT mice.

Table 2. Tukey's multiple comparisons tests performed on INSRα-B in TgSwDI and WT mice with corresponding p-values.

INSRα-B	**P-value**
Total brain (TgSwDI) vs. capillaries (TgSwDI)	0.0362
Total brain (TgSwDI) vs. brain fraction (TgSwDI)	0.0002
Capillaries (TgSwDI) vs. brain fraction (TgSwDI)	0.0005
Total brain (WT) vs. capillaries (WT)	0.0096
Total brain (WT) vs. brain fraction (WT)	0.0003
Capillaries (WT) vs. brain fraction (WT)	0.0008

Unpaired statistical tests were performed to compare expression levels of INSRα-A and INSRα-B in the three samples between TgSwDI and WT mice (Fig. 11A and B). Both datasets were analyzed using one-way ANOVA, followed by Dunnett's T3 multiple comparisons test. No significant differences in total brain and isolated capillary fractions between TgSwDI and WT mice were found. Additionally, a significant increase in both INSRα-A ($p = 0.0245$) and INSRα-B ($p = 0.0062$) was identified in brain fraction samples in TgSwDI mice compared to WT mice (Fig. 11A and B). Expression levels of INSRα-A and INSRα-B in the isolated capillary fractions were further analyzed by dividing the mice according to age (Fig. 11C and D). The age-divided groups were compared by using one-way ANOVA. No significant differences in both INSRα-A and INSRα-B in isolated capillary fractions were found between TgSwDI mice aged 18 and 30 months and WT mice aged 12 months (Fig. 11C and D). The INSRα-A/B ratio from each mouse

was calculated to further compare the INSRα-A/B ratio in isolated capillary fractions between TgSwDI and WT mice (Fig. 11E). The Mann-Whitney U test was applied, and the INSRα-A/B ratio in isolated capillary fractions between TgSwDI and WT mice was found to be non-significant (p >0.05) (Fig. 11E). To summarize, comparisons of TgSwDI and WT mice showed no significant differences in total brain and isolated capillary fractions. However, the opposite was examined for both INSRα-A and INSRα-B in brain fractions between the two groups of mice. Furthermore, no significant differences of INSRα-A and INSRα-B in isolated capillary fractions were determined by dividing the mice according to age. Similarly, results were identified by calculation of the INSRα-A/B ratio of each mouse.

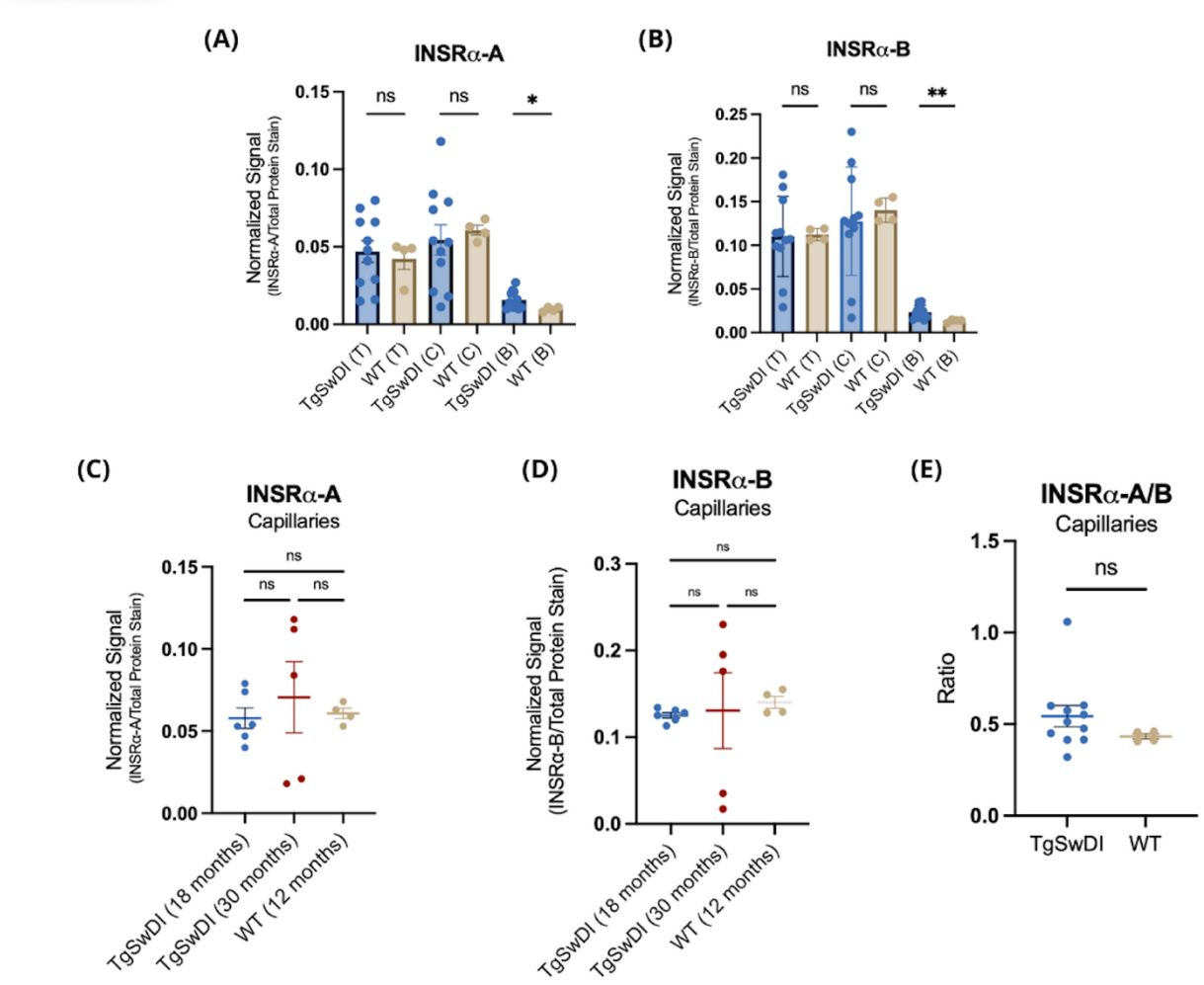

Fig. 11. (A and B) Scattered bar plots of normalized signal values for INSRα-A and INSRα-B in total brain and isolated capillary and brain fractions for TgSwDI and wild-type mice. Brain fractions from TgSwDI mice showed a significant increase in INSRα-A (p = 0.0245) and INSRα-B (p = 0.0062) compared to brain

*fractions from wild-type mice. (C and D) Dot plots of normalized signal values for INSRα-A and INSRα-B in isolated capillary fractions for TgSwDI (18 months), TgSwDI (30 months) and wild-type (12 months) mice. The analyses showed no significant differences between the age-dependent groups (p >0.05). (E) Dot plot of the calculated INSRα-A/B ratio in TgSwDI and WT mice, showing non-significant data (p >0.05). Data depicted as mean ± SEM and analyzed with Welch ANOVA test followed by Dunnett's multiple comparisons test, n = 15 (A-B), the one-way ANOVA followed by Tukey's multiple comparisons test, n = 15 (C-D) or the Mann-Whitney U test, n = 15 (E). *p <0.05, **p <0.01. T: Total brain, C: Capillaries, B: Brain fraction, INSR: Insulin receptor, WT: Wild type, ns: Non-significant.*

3.4 Protein Content of IGF-1R

WB analyses allowed identification of IGF-1R at ~200 kDa following the datasheet of the IGF-1R antibody (Fig. 12A). An overview of the WB bands identifying IGF-1R is shown in Appendix A.2. Several protein concentrations were blotted on a membrane to determine the most optimal concentration for investigation of the expression levels of IGF-1R (Fig. 12A). It was observed that accurate identification of WB bands was obtained by using a high protein concentration. Therefore, to quantify the expression levels of IGF-1R, 50 μg of protein was loaded on the gels performed in this project. Since 12 μL was loaded into each well, and the brain fraction samples consisted of minimal protein concentrations, the loading of these samples would exceed the total volume. Consequently, it was not possible to analyze the brain fraction samples. For this reason, samples used to assess IGF-1R expression levels were limited to total brain and isolated capillary fractions. As previously described, a linear range of detection was conducted by staining a membrane with total protein stain containing different protein concentrations (30-60 μg) of the target protein (Fig. 12B). The combined linear range of the target protein and the total protein stain was analyzed to determine the most suitable range of protein to load on the gels (Fig. 12C). A protein concentration of 50 μg does not fall within the green segments for both the target protein and total protein stain. However, the combined linear range falls within an acceptable range (Fig. 12C). The signal values for IGF-1R were examined to be low (Fig. 12C), further supporting the conclusion of loading 50 μg of protein on the gels.

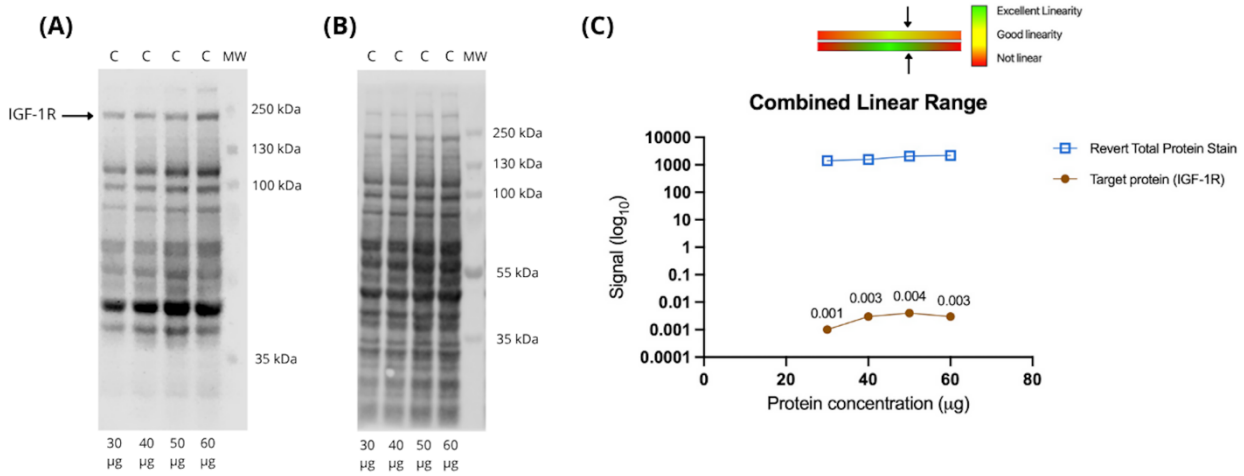

Fig. 12. (A) Western blot analyses of IGF-1R revealed bands at ~200 kDa following the datasheet of the IGF-1R antibody [86]. (B) Multiple protein concentrations *(30 µg, 40 µg, 50 µg and 60 µg)* were blotted on a membrane stained with *total protein stain to perform a linear range of detection. (C) The calculated combined linear range between the target protein and total protein stain.* 50 *µg* protein does not fall within the green segments for both the target protein and total protein stain but appears to fall within an *acceptable detection range. C: Capillaries, MW: Molecular weight. IGF-1R: Insulin-like growth factor 1 receptor.*

To determine the most suitable antibody concentration of IGF-1R, two different antibody concentrations were tested (1:200 and 1:500) (Fig. 13A). Since an antibody concentration of 1:500 did not allow clear identification of IGF-1R, it was concluded that 1:200 was the most optimal antibody concentration to use (Fig. 13A). Therefore, an antibody concentration of 1:200 was used in all WBs detecting IGF-1R. Although IGF-1R was identified at the expected molecular weight (~200 kDa), several bands of varying sizes were presented across the blots (Appendix A.2). To investigate further if these bands could be reduced, decreased antibody concentrations were validated (1:500 and 1:800) (Fig. 13B). This time, decreased antibody concentrations produced a more detective target band of IGF-1R, suggesting that the previous test of the antibody concentrations may have been affected by inexperience with the procedure. However, reduced antibody concentrations appeared to have only a slight effect on non-specific bands across the blots (Fig. 13B).

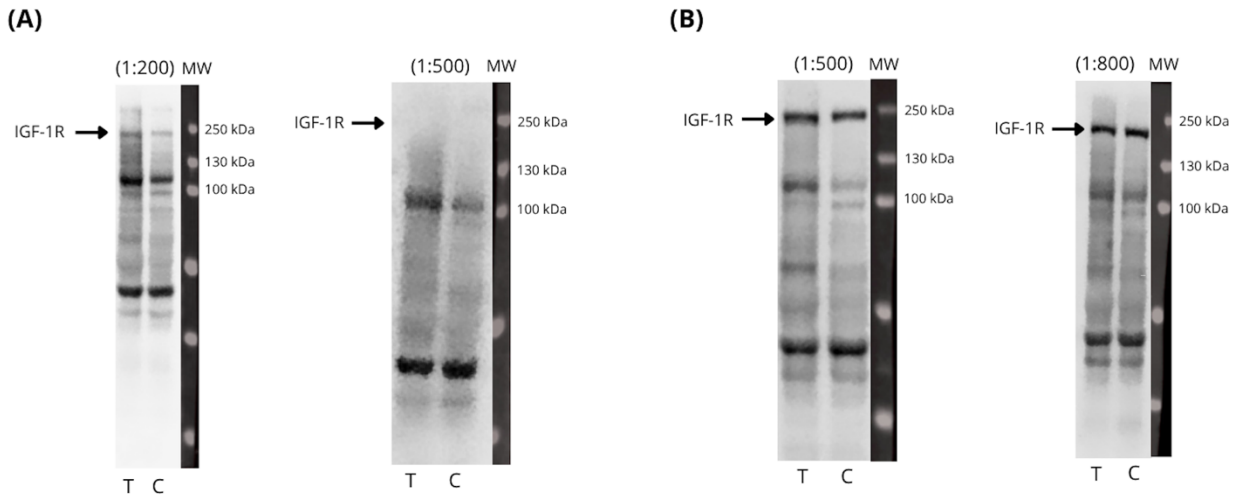

Fig. 13. (A) Different antibody concentrations (1:200 and 1:500) were investigated to determine the optimal antibody concentration of IGF-1R. An antibody concentration of 1:500 did not allow the identification of IGF-1R. Therefore, an antibody concentration of 1:200 was used in this project. (B) Non-specific Western blot bands were investigated by using decreased antibody concentrations (1:500 and 1:800). This resulted in improved detection of IGF-1R, whereas it did not appear to reduce non-specific bands. T: Total brain, C: Capillaries, MW: Molecular weight.

Visualization of the WB bands showed a slight increase in the signal intensities of IGF-1R in TgSwDI mice compared to WT mice for both total brain and isolated capillary fractions (Fig. 14A and Appendix A.2). Statistical comparisons between expression levels of IGF-1R in total brain and isolated capillary fractions within each mouse were conducted using paired tests (Fig. 14B and C). Both datasets from TgSwDI and WT mice were analyzed using the Wilcoxon matched-pairs signed rank test. No significant differences ($p > 0.05$) were found between total brain and isolated capillary fractions within each mouse for TgSwDI and WT mice (Fig. 14B and C). Unpaired statistical tests were performed to compare expression levels of IGF-1R in total brain and isolated capillary fractions between TgSwDI and WT mice (Fig. 14D and E). The Mann-Whitney U test was performed for both datasets, showing significant differences ($p < 0.05$) between TgSwDI and WT mice in total brain and isolated capillary fractions (Fig. 14D-E and Table 3).

Table 3. Mann-Whitney U test performed on IGF-1R in total brain and isolated capillary fractions between TgSwDI and WT mice with corresponding p-values:

IGF-1Rα	**P-value**
Total brain (TgSwDI) vs. Total brain (WT)	0.0300
Capillaries (TgSwDI) vs. Capillaries (WT)	0.0022

Table 4. Dunn's multiple comparisons test performed on IGF-1R in total brain and isolated capillary fractions between TgSwDI (18 months) and WT mice (12 months) with corresponding p-values:

IGF-1Rα	**P-value**
Total brain (TgSwDI, 18 months) vs. Total brain (WT, 12 months)	0.0255
Capillaries (TgSwDI, 18 months) vs. Capillaries brain (WT, 12 months)	0.0195

Comparisons between TgSwDI and WT mice were further conducted by dividing the mice according to age (Fig. 14F and G). The Kruskal-Wallis test was applied, followed by Dunn's multiple comparisons test. A significant increase ($p < 0.05$) in the expression levels of IGF-1R was observed for both total brain and isolated capillary fractions in TgSwDI mice aged 18 months compared to WT mice aged 12 months (Table 4). However, no significant differences were identified between the remaining groups (Fig. 14F and G). Overall, no significant differences in IGF-1R were detected between total brain and isolated capillary fractions within each mouse of TgSwDI and WT mice. In addition, significant differences of IGF-1R between TgSwDI and WT in both total brain and isolated capillary fractions were reported. By comparing TgSwDI mice aged 18 months and WT mice aged 12 months, a significant difference in total brain and isolated capillary fractions were detected.

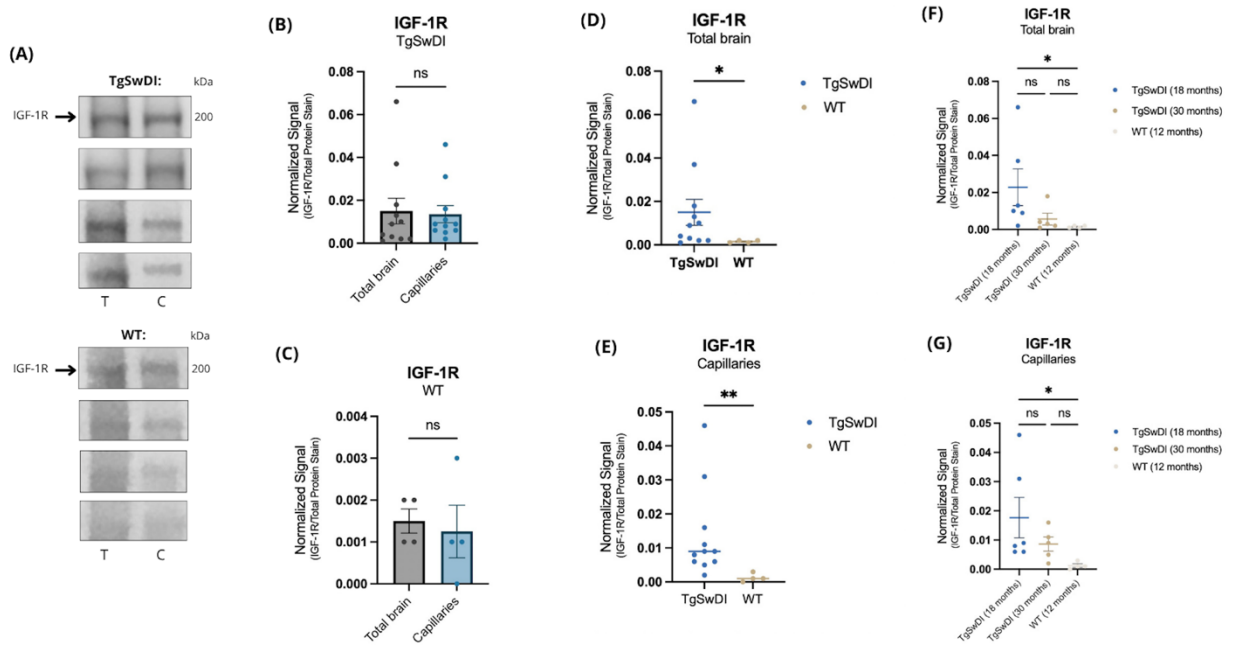

*Fig. 14. (A). Identification of IGF-1R (~200 kDa) on representative Western blots for TgSwDI and wild-type mice. (B and C) Scattered bar plots of normalized signal values for IGF-1R in total brain and isolated capillary fractions for TgSwDI and wild-type mice showed no significant differences (p >0.05). (D and E) Dot plots showing normalized signal values for IGF-1R in total brain and isolated capillary fractions between TgSwDI and WT mice. A significant increase in the expression levels of IGF-1R in total brain and isolated capillary fractions was observed in TgSwDI mice compared to wild-type mice (Table 3). (F and G) Dot plots illustrating normalized signal values for IGF-1R in total brain and isolated capillary fractions between TgSwDI (18 months), TgSwDI (30 months) and wild-type (12 months) mice. Significant differences were detected between TgSwDI mice aged 18 months and wild-type mice aged 12 months in both total brain and isolated capillary fractions (Table 4). Data depicted as mean ± SEM and analyzed with Wilcoxon matched-pairs signed rank test, n = 11 (B), n = 4 (C), Mann-Whitney U test, n = 15 (D and E) or the Kruskal-Wallis test, n = 15 (F and G). *p <0.05, **p <0.01. T: Total brain, C: Capillaries, WT: Wild-type, ns: Non-significant.*

3.5 Phosphorylation Levels of IGF-1Rβ/INSRβ

P-IGF-1Rβ/INSRβ was identified at ~95 kDa following the datasheet of the antibody [87] (Fig. 15A). An overview of the WB bands analyzing p-IGF-1Rβ/INSRβ can be found in Appendix A.3. Quantification of p-IGF-1Rβ/INSRβ required a high protein concentration (Fig. 15A). To obtain

the most visible WB bands, 50 μg of protein was loaded on the gels. Comparable to IGF-1R, low protein concentrations were detected in the brain fraction samples used for the investigation of p-IGF-1Rβ/INSRβ. Therefore, an examination of p-IGF-1Rβ/INSRβ was performed on the total brain and isolated capillary fractions. A combined linear range of the target protein and total protein stain was assessed (Fig. 15B). Although a protein concentration of 50 μg did not fall within green segments, the combined linear range appeared to fall within an acceptable range of detection (Fig. 15B). Similarly to IGF-1R, non-specific bands of different sizes were observed across the blots in addition to the target band (Appendix A.3). A control blot without addition of the primary antibody was performed. No bands were detected, suggesting that non-specific bands were due to the primary antibody. WB analyses of p-IGF-1Rβ/INSRβ were conducted using an antibody concentration of 1:1000, following the datasheet provided by the antibody [87]. To investigate if a decreased antibody concentration may reduce non-specific bands on the blots, two different antibody concentrations (1:1200 and 1:1500) were applied (Fig. 15C). By using decreased antibody concentrations, the bands were not detectable, supporting the conclusion of using a higher antibody concentration.

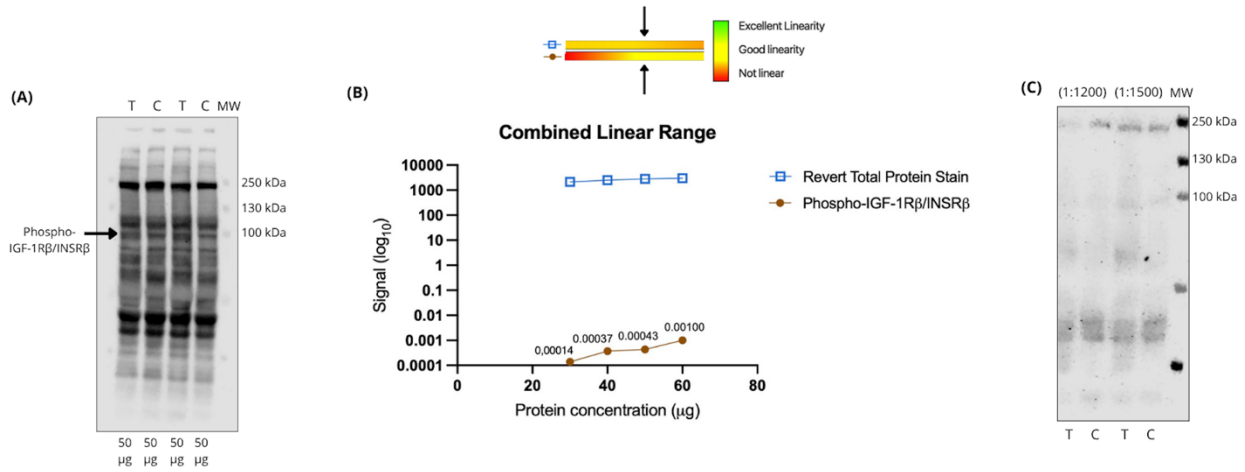

Fig. 15. (A) Identification of phospho-IGF-1Rβ/INSRβ (~95 kDa) [87] on a representative Western blot. (B) Illustration of the combined linear range between the target protein and total protein stain. 50 μg of protein was concluded to fall within an acceptable range of detection. Signal values for *phosphor-IGF-1Rβ/INSRβ were found to be low, supporting the decision of loading a high protein concentration on the gels. (C) Test of different antibody concentrations of phosphor-IGF-1Rβ/INSRβ (1:1200 and 1:1500). No*

visible bands were detected, supporting the decision of using an antibody concentration of 1:1000. T: Total brain, C: Capillaries, MW: Molecular weight.

WB bands of p-IGF-1Rβ/INSRβ were characterized by low signal intensities (Fig. 16A). No band signals were observed in total brain samples from TgSwDI mice exposed to insulin injections (Fig. 16B). To compare normalized signal values for TgSwDI and WT mice receiving insulin and saline, a Kruskal-Wallis test of total brain and isolated capillary fractions was performed (Fig. 16B and C). For both total brain and isolated capillary fractions, Dunn's multiple comparisons test was not able to observe any significant differences between the groups ($p > 0.05$) (Fig. 16B and C).

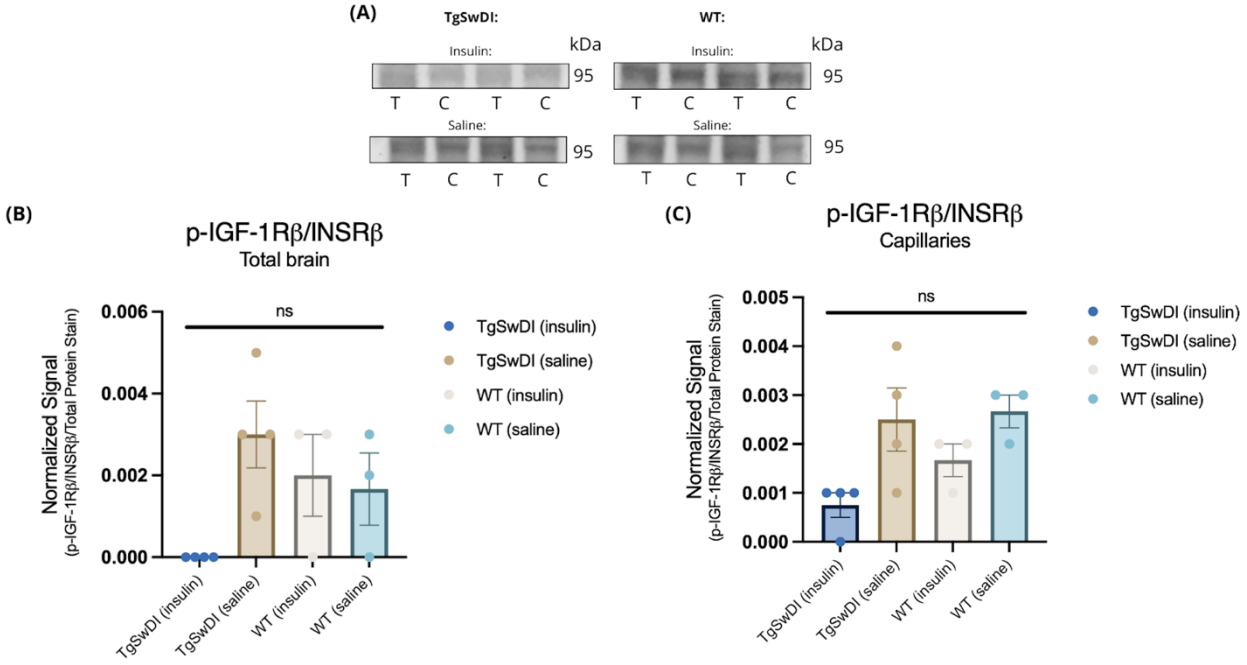

Fig. 16. (A) Representative Western blots of phospho-IGF-1Rβ/INSRβ in TgSwDI and wild-type mice exposed to insulin and saline injections. The band intensities were observed to be low. (B and C) Scattered bar plots of normalized signal values for TgSwDI and wild-type mice receiving insulin and saline in total brain and isolated capillary fractions. No significant differences between the groups were seen ($p > 0.05$). Data depicted as mean $\pm$ SEM and analyzed with Kruskal-Wallis test, n = 14 (B and C). T: Total brain, C: Capillaries, WT: Wild-type.

4. Discussion

In light of the findings presented above, the following discussion will focus on the location, expression and phosphorylation levels of INSR and IGF-1R, which serve as characteristic features in the investigation of BIR. Furthermore, WB analyses will be discussed as the chosen methodological approach to investigating BIR.

4.1 WB Procedure

Overall, changes in the protein content of the INSR signaling pathway are often used to characterize and define BIR [10]. WB analyses are the most widely applied and reliable methods to investigate the INSR signaling pathway [10]. The technical procedure for WB analyses includes an internal loading control (ILC) used to confirm equal sample loading across all wells [92]. Housekeeping proteins (HKPs), such as Actin and glyceraldehyde-3-phosphate dehydrogenase (GAPDH), are widely used ILCs. Evidence suggests that HKPs are accurate but may be vulnerable to biological variation [92], [93]. Currently, total protein staining of blotted membranes has been the most favored method for normalization of sample loading [92]. Total protein staining is more resistant to biological variability and may display a wider linear range of detection compared to HKPs [92], [93]. Therefore, Revert™ 700 Total Protein Stain (LI-COR) was used as an ILC in this project. The linear range of detection is essential for accurate quantitative WB analyses [92], [94]. Within the linear range of detection, a proportional relationship between band intensity and the amount of target protein is displayed [92], [94]. Outside the linear range, the signal intensity is not determined by sample loading and does not reflect the exact amount of target protein [92], [94]. The combined linear range is used to identify a proper level of sample to load, resulting in a linear response for both the target protein and total protein stain [94]. Determining the linear range of detection should be conducted before WB analyses of the samples. In this case, the linear range of detection was performed following WB analyses. As a result, the linear range of detection served as quality control to ensure that a proper amount of target protein was loaded. 25 or 50 μg of protein was loaded on the gels to investigate protein levels of either the INSRα isoforms or IGF-1R. Following the linear range of detection, a loading concentration of 22 μg would have been the most

suitable amount to load to investigate the INSRα isoforms, along with 45 μg of protein in detecting IGF-1R. INSRβ/IGF-1Rβ phosphorylation levels were assessed using 50 μg of protein, and the combined linear range falls within yellow segments by loading 45-50 μg of protein. Outside of these ranges, a reduced linearity begins to occur. In conclusion, none of the protein concentrations loaded in this project revealed that both the target protein and total protein stain were detectable within green segments of the combined linear range. However, overlapping segments of yellow indicate accurate detection of the target protein and total protein stain [95]. Additionally, examination of the linear range of detection before WB analyses would have strengthened the results.

WB analyses displayed low signal intensities of both IGF-1R and p-IGF-R1β/INSRβ. As previously described, due to limited protein concentrations, brain fraction samples were not included in the investigation of IGF-1R and p-IGF-R1β/INSRβ. Preparation of brain fraction samples was conducted through two centrifugation steps to separate the brain "cake" from the remaining sample. This procedure may have led to the loss of total proteins in the samples. Low signal intensities of the target proteins could potentially be enhanced through further antibody optimization. This was observed for IGF-1R while validating proper antibody concentration, as described earlier. To improve the detection of low signal intensities in WB analyses, another chemiluminescent HRP substrate could have been applied. The SuperSignal™ West Dura Extended Duration Substrate (34075, Thermo Fisher Scientific) is thought to display the best signal duration and is primarily used when the target protein is less abundant [96].

Another characteristic feature of WB analyses of IGF-1R and p-IGF-1Rβ/INSRβ was the presence of non-specific bands across the blots. This observation could be attributed to various factors. Firstly, excessively high protein loading could result in the presence of non-specific bands [97]. As previously specified, protein concentrations loaded for IGF-1R and p-IGF-1Rβ/INSRβ fell within segments showing good linearity in the combined linear range. However, protein loading for both IGF-1R and p-IGF-1Rβ/INSRβ could have been slightly reduced by adding 45 μg instead of 50 μg. Secondly, using an abnormally high antibody

concentration could lead to non-specific bands [97]. However, the addition of a reduced antibody concentration of IGF-1R in this project appeared to have a minimal effect on the presence of non-specific bands. WB analysis of p-IGF-1Rβ/INSRβ without adding the primary antibody was conducted. The results suggested that non-specific bands were primarily driven by the primary antibody rather than the secondary antibody. Using a lower antibody concentration of p-IGF-1Rβ/INSRβ was not possible due to non-detectable bands. Additionally, methodological adjustments such as changing the blocking/washing strategy and increasing the duration and number of washes should be considered [98]. Membranes used to detect IGF-1R and p-IGF-1Rβ/INSRβ were blocked using 1X PBS containing 3% skim milk powder and 2% Tween 20. The membranes were further washed and incubated with antibodies in 1X PBS containing 0,05% Tween 20. This procedure was conducted according to a previous study [84]. A study by Yan et al. investigated the expression levels of IGF-1R in mice during a bowel necrotic disease using a similar IGF-1R antibody as used in this project [99]. The blocking strategy performed by Yan and co-workers included 5% milk containing Tween 20 [99]. Another study by Rodriguez et al. used a similar p-IGF-1Rβ/INSRβ antibody as used in this project to examine how the downregulation of s-resistin affects insulin signaling in Wistar rats [100]. WB analyses were executed using 1X PBS containing 0,05% Tween 20 and 5% milk powder for antibody incubation [100]. In conclusion, these findings suggest that no standardized protocol for WB analyses exists. Blots of INSRα isoforms conducted in this project were characterized by a lower presence of non-specific bands. These membranes were blocked using 1X PBS containing 3% Tween 20. This blocking method could have been tested on blots of IGF-1R and p-IGF-1Rβ/INSRβ as well to determine if the presence of non-specific bands was minimized.

4.2 Location of INSR

Various studies suggest that INSR is particularly concentrated at the BBB [42], [56], [101], [102], [103], [104]. Similar findings were demonstrated in this project. Protein levels of INSRα-B in isolated capillary fractions were significantly increased compared to total brain and brain fraction samples in both TgSwDI and WT mice. A similar observation was identified of INSRα-A in TgSwDI mice. Cresyl violet staining confirmed the enrichment of vascular structures in the

isolated capillary fractions compared to the brain fraction samples. These findings suggest that the brain capillary depletion technique was reliable.

4.3 Protein Content of INSR

Previously published data suggested that AD is associated with reduced expression levels of INSRs in the brain [24], [42], [56], [105], [106]. As early as 2005, Monte et al. found a significant reduction in the number of INSRs in postmortem brain tissues from AD patients [24]. This reduction was particularly identified in the frontal cortex, hippocampus and hypothalamus [24]. Since then, these findings have been replicated in a study by Liu et al., demonstrating similar results [106]. Overall, Calon and colleagues primarily detected INSRα-B in vascular fractions, as INSRα-B was virtually absent in the brain parenchyma and whole brain homogenates [56]. This project examined no significant differences in INSRα-A and INSRα-B between TgSwDI and WT mice in total brain and isolated capillary fractions. However, a significant increase in the protein content of INSRα-A and INSRα-B was found in brain fraction samples in TgSwDI mice compared to WT mice. In contrast to the study conducted by Calon et al. [56], this project found high protein levels of INSRα-B in both total brain and isolated capillary fractions, and to a lesser extent, in the brain fraction samples. These contrasting findings may result from various factors. Additionally, research by Calon et al. identified a lower INSRα-A/B ratio in brain microvessels in mice than humans [56]. This finding suggests that an altered INSRα-A/B ratio may be more challenging to assess in the mouse brain. Therefore, applying human brain tissues to this project could provide new insights into the INSRα-A/B ratio. Moreover, a key strength of the study conducted by Calon et al. was the high number of human control brains (n = 20) and non-Tg mice (n = 39) used for the investigation of the INSRα isoforms [56]. Conversely, this project used a markedly lower number of WT mice (n =4) to detect the INSRα isoforms. This could potentially explain the non-significant observations of INSRα isoforms between TgSwDI and WT mice in total brain and isolated capillary and brain fractions. An increased number of control mice could strengthen the findings of this project. Although this project did not replicate the study's results by Calon et al., similar findings have been reported in previous studies [12], [23]. A study by Talbot et al. demonstrated normal levels

of INSRβ in the cerebellar cortex and hippocampus in AD brains compared to controls [12]. Additionally, decreased responses to insulin in the PI3K signaling pathway were observed in AD brains following ex vivo insulin stimulation [12]. These findings by Talbot and colleagues indicate that impairments in the insulin signaling pathway were mainly detectable in the activation states of the signaling molecules [12]. Another study by Moloney et al. investigated the expression levels of INSRα and INSRβ in AD patients compared to controls using WB and immunofluorescent microscopy [23]. This study concludes similarly expression levels of INSRα and INSRβ between AD patients and controls [23].

Another crucial factor to consider when investigating INSRα isoforms is aging. Evidence suggests that insulin sensitivity and expression levels of INSR progressively decrease with age [1], [105]. Calon et al. investigated vascular levels of INSRα-B in 3xTg-AD and Non-Tg mice aged 6, 12 and 18 months [56]. From 6 to 18 months, a significantly decreased linear trend of INSRα-B was calculated in 3xTg-AD mice, suggesting that the levels of INSRα-B are reduced with age [56]. The 3xTg-AD mouse model used by Calon et al. [56] to investigate INSRα isoforms is supported by evidence from previous studies. Griffith et al. showed that 3xTg-AD mice at an age of 1 month exhibit impaired glucose tolerance [107]. Moreover, Chen et al. found that daily intranasal injection of insulin restored insulin signaling and reduced Aβ40 levels in the brains of 3xTg-AD mice [108]. In addition, this project aimed to investigate whether the levels of INSRα isoforms decrease with age in a TgSwDI mouse model of AD. By comparing TgSwDI mice aged 18 and 30 months and WT mice aged 12 months, no significant differences in INSRα isoforms were detected in the isolated capillary fractions. The data of TgSwDI mice aged 30 months showed high variability. Based on the available literature, no studies have currently determined the role of insulin signaling in the TgSwDI mouse model of AD. Therefore, whether this model is less sensitive to insulin signaling remains unclear. Since Aβ accumulation in TgSwDI mice begins early with widespread deposits by 12 months, neurodegeneration and tissue damage may vary between mice at 30 months used in this project. This suggests that the data variability observed in TgSwDI mice aged 30 months may reflect biological heterogeneity between the mice.

4.4 Location of IGF-1R

This project aimed to investigate the location of IGF-1R in the mouse brain. No significant difference between total brain and isolated capillary fractions was observed in TgSwDI and WT mice. Growing evidence suggests that IGF-1R is widely distributed in BECs and isolated brain microvessels [70], [102], [103], [104], [109]. A recent study by Zhang et al. analyzed expression levels of IGF-1R in isolated brain microvessels, brain parenchyma and peripheral organs of mice and humans using an RNA-seq approach [109]. Zhang and colleagues observed high expression levels of IGF-1R in mouse brain microvessels compared to peripheral tissues [109]. Compared to humans, a significantly higher level of IGF-1R was identified in the brain microvessels of mice [109]. Generally, evidence supporting the exact location of IGF-1R in the brain remains limited. The inclusion of brain fraction samples in this project would have strengthened the results and potentially given new insights into this research area.

4.5 Protein Content of IGF-1R

Protein levels of IGF-1R in TgSwDI mice were found to be markedly increased in both total brain ($p = 0.0300$) and isolated capillary fractions ($p = 0.0022$) compared to WT mice. Conflicting data exist regarding the association between AD and expression levels of IGF-1R in the brain. Several studies support the findings from this project by identifying increased IGF-1R levels in AD brains [23], [71]. A study by Selles et al. observed increased IGF-1R levels in postmortem hippocampal tissue from AD patients [71]. Furthermore, Moloney et al. detected increased IGF-1R levels in the temporal cortex of AD patients both surrounding and within Aβ plaques [23]. However, a significantly reduced number of neurons expressing IGF-1R in AD was detected [23]. Recent studies showed that reduced IGF signaling in the brain leads to decreased Aβ pathology, neuroinflammation and neurodegeneration in mouse models of AD [73], [74]. IGF-1 is considered to inhibit autophagy [73], [74]. Therefore, decreased IGF-signaling will support autophagy in neurons and remove toxic Aβ oligopeptides [73], [74]. A study by Bale et al. investigated the inhibition of a metalloprotease, PAPP-A, which is responsible for the

bioavailability of IGF-1 by cleaving IGFBPs [72]. This study demonstrated that AD/PAPPA-A knock-out mice showed significantly reduced Aβ plaque burden, improved cognitive behavior and lower IGF-1 activity [72]. Therefore, suppressing IGF-1R signaling may reduce the progression of AD. However, IGF-1R plays a key role in growth and metabolism, which makes it impractical to inhibit [72]. In contrast to these findings, the study by Monte et al. found markedly reduced expression levels of IGF-1R in AD patients [24]. Additional data by Monte and co-workers reported that advanced AD brains were characterized by reduced IGF-1R expression [24]. Generally, the progression through the Braak stages has been linked to a reduction in the levels of IGF-1, IGF-2 and their receptors [24]. This project detected a similar observation by comparing TgSwDI mice (18 and 30 months) and WT mice (12 months). Data showed that TgSwDI mice aged 30 months tended to express lower IGF-1R levels compared to TgSwDI mice aged 18 months, although differences were non-significant.

4.6 Phosphorylation Levels of IGF-1Rβ/INSRβ

INSR activation by injection of insulin in the blood circulation of mice can be challenging [10]. BBB transport of insulin is saturable, suggesting that once the saturable rate is reached, increased injection of insulin does not enhance the levels in the brain [10]. Studies investigating this research area vary in terms of factors such as administration, brain region analyzed and type/dosage of insulin [10]. Minimal studies directly measured INSR or IRS-1 phosphorylation in rodent models [110], [111], [112], [113], which may be due to a limited number of reliable antibodies [10]. Instead, several studies examined phosphorylation levels of downstream kinases such as Akt, GSK3β or Erk1/2 [114], [115], [116], [117], [118], [119]. Although the activation of the Akt/GSK3β/Erk1/2 pathway is more widely measured, the phosphorylation of INSRβ displays the initial activation step following insulin binding [10], [42]. In contrast, downstream kinases are shared by a wide variety of cell signaling pathways, making it difficult to link the phosphorylation levels to a specific response to insulin [10], [42]. Therefore, this project aimed to investigate the direct phosphorylation of IGF-1Rβ/INSRβ. However, this project did not detect any differences between TgSwDI and WT mice receiving insulin or saline in total brain and isolated capillary fractions. Higher phosphorylation levels following saline

injection compared to insulin suggested a methodological issue. The experimental procedure of insulin injection was performed as conducted in a previous study by Jiang et al. [116]. After 2 hours of fasting, IP injection of insulin (5 I.U./kg) was performed in C57BL/6 mice [116]. The mice were sacrificed at 5, 15, 30 and 60 minutes after IP injection [116]. Jiang and co-workers found an activation of the PI3K-Akt signaling pathway in the liver immediately after insulin injection [116]. In contrast, activation of the PI3K-Akt signaling pathway in the brain was observed to be increased at longer time points (30-60 minutes) [116]. Based on this study, this project expected that phosphorylation of IGF-1Rβ/INSRβ would occur following 30 minutes of IP insulin injection. In contrast, other studies have reported different results. A study by Muller et al. found increased phosphorylation of INSRβ at 15 minutes following insulin injections [120]. Overall, several studies suggest that the activation of the downstream cascade of INSR is fast, and phosphorylation of Akt within 15 minutes after insulin injection has been demonstrated [115], [116], [119], [120]. These findings suggest that 15 minutes may have been the preferred time point to investigate phosphorylation levels of INSRβ following insulin injections. Generally, limited studies have identified phosphorylation of INSRβ after insulin injection [56], [120]. These studies performed insulin injections through intracerebroventricular or intracarotid routes [56], [120]. Additionally, the study by Calon et al. showed that INSRβ phosphorylation can be detected in microvessels using intracarotid injection of insulin [56]. Therefore, an alternative method of insulin injections in this project should be considered. As provided earlier, no studies have currently reported the role of insulin injections in the TgSwDI mouse model of AD. Therefore, it remains unclear whether INSR activation can be demonstrated in this model.

4.7 Perspective

Research demonstrates that brain glucose metabolism may begin to decline more than 10 years before dementia symptoms appear [1], suggesting that a better understanding of BIR could contribute to the early detection of AD. Further research determining the exact underlying mechanisms and location of BIR in the brain is essential for developing more effective targeted treatment options in the future. Additionally, since T2DM and BIR share similar characteristics,

overlapping treatment options may be possible [19]. The INSR and IGF-1R signaling pathways represent two complex and distinct pathways. However, increasing evidence suggests that their interplay may be important for further research of BIR in AD [76]. In recent years, the presence of HybRs has gained increased attention [76]. Data suggests that if either INSR or IGF-1R is present in lower amounts, it is more likely to form HybRs rather than homodimers [45], [76]. HybRs exert a low affinity for insulin, leading to reduced insulin sensitivity [76]. In a study by Fernández et al., overexpression of the dominant-negative IGF-1R in the skeletal muscle of mice led to the incorporation of INSRs into HybRs, resulting in insulin resistance [79]. As previously reported, several studies suggest that early stages of AD are characterized by decreased INSR levels, while IGF-1R levels are increased. Considering this, it would potentially lead to the incorporation of INSRs into HybRs and the development of BIR. To confirm or disconfirm this mechanism, further research on the formation of HybRs in the brains of AD patients and their potential role in the development of BIR is needed.

5. Conclusion

This project provides new insights into BIR by investigating INSR and IGF-1R signaling in an experimental (TgSwDI) mouse model of AD. To determine expression and phosphorylation levels of INSR and IGF-1R at the level of the BBB, three samples from each mouse were obtained, including total brain and isolated capillary and brain fractions. INSRα-A and INSRα-B were mainly concentrated in the isolated capillary fractions rather than in total brain and brain fraction samples. A higher vascular INSRα-A/B ratio was previously reported as a molecular index of BIR in the study by Calon et al. In contrast, this project did not demonstrate reduced levels of INSRα-B in the isolated capillary fractions, resulting in a higher INSRα-A/B ratio. Due to low protein concentrations of the brain fraction samples, the enrichment of IGF-1R in the isolated capillary fractions compared to capillary-depleted brain fractions could not be determined. In addition, expression levels of IGF-1R were increased in TgSwDI mice compared to WT mice. Although a declining tendency in the protein levels of IGF-1R in TgSwDI mice was observed with increasing age, the difference was not statistically significant. The phosphorylation levels of INSR and IGF-1R showed no significant differences between TgSwDI and WT mice. The roles of INSR and IGF-1R signaling in AD remains unclear, highlighting the need for further research to characterize BIR. Further research, investigating the underlying mechanisms of BIR and identification of where BIR arise in the brain, may be necessary to understand the cause of AD.

References

[1] J. H. Yoon *et al.*, "How Can Insulin Resistance Cause Alzheimer's Disease?," *Int J Mol Sci*, vol. 24, no. 4, p. 3506, Feb. 2023, doi: 10.3390/IJMS24043506.

[2] C. Qiu, M. Kivipelto, and E. Von Strauss, "Epidemiology of Alzheimer's disease: occurrence, determinants, and strategies toward intervention," *Dialogues Clin Neurosci*, vol. 11, no. 2, p. 111, 2009, doi: 10.31887/DCNS.2009.11.2/CQIU.

[3] World Health Organization, "Dementia." Accessed: Apr. 22, 2025. [Online]. Available: https://www.who.int/news-room/fact-sheets/detail/dementia

[4] Videnscenter for demens, "Dementia in Denmark | Nationalt Videnscenter for Demens." Accessed: Apr. 22, 2025. [Online]. Available: https://videnscenterfordemens.dk/en/dementia-denmark

[5] P. T. Kamatham, R. Shukla, D. K. Khatri, and L. K. Vora, "Pathogenesis, diagnostics, and therapeutics for Alzheimer's disease: Breaking the memory barrier," *Ageing Res Rev*, vol. 101, p. 102481, Nov. 2024, doi: 10.1016/J.ARR.2024.102481.

[6] D. M. Holtzman, J. C. Morris, and A. M. Goate, "Alzheimer's Disease: The Challenge of the Second Century," *Sci Transl Med*, vol. 3, no. 77, p. 77sr1, Apr. 2011, doi: 10.1126/SCITRANSLMED.3002369.

[7] S. M. De la Monte, "Type 3 diabetes is sporadic Alzheimer's disease: Mini-review," *European Neuropsychopharmacology*, vol. 24, no. 12, pp. 1954–1960, Dec. 2014, doi: 10.1016/J.EURONEURO.2014.06.008.

[8] I. Pomytkin and V. Pinelis, "Brain Insulin Resistance: Focus on Insulin Receptor-Mitochondria Interactions," *Life 2021, Vol. 11, Page 262*, vol. 11, no. 3, p. 262, Mar. 2021, doi: 10.3390/LIFE11030262.

[9] S. E. Arnold *et al.*, "Brain insulin resistance in type 2 diabetes and Alzheimer disease: concepts and conundrums," *Nat Rev Neurol*, vol. 14, no. 3, p. 168, Mar. 2018, doi: 10.1038/NRNEUROL.2017.185.

[10] E. M. Rhea *et al.*, "State of the Science on Brain Insulin Resistance and Cognitive Decline Due to Alzheimer's Disease," *Aging Dis*, vol. 15, no. 4, p. 1688, Aug. 2024, doi: 10.14336/AD.2023.0814.

[11] M. Maciejczyk, E. Żebrowska, and A. Chabowski, "Insulin Resistance and Oxidative Stress in the Brain: What's New?," *International Journal of Molecular Sciences 2019, Vol. 20, Page 874*, vol. 20, no. 4, p. 874, Feb. 2019, doi: 10.3390/IJMS20040874.

[12] K. Talbot *et al.*, “Demonstrated brain insulin resistance in Alzheimer’s disease patients is associated with IGF-1 resistance, IRS-1 dysregulation, and cognitive decline,” *J Clin Invest*, vol. 122, no. 4, p. 1316, Apr. 2012, doi: 10.1172/JCI59903.

[13] K. Talbot and T. Org, “Brain insulin resistance in Alzheimer’s disease and its potential treatment with GLP-1 analogs,” *Neurodegener Dis Manag*, vol. 4, no. 1, p. 31, 2014, doi: 10.2217/NMT.13.73.

[14] A. S ̨ Edzikowska, L. Szablewski, A. A. Rostagno, A. Baranowska-Bik, and A. Orzechowski, “Insulin and Insulin Resistance in Alzheimer’s Disease,” *Int J Mol Sci*, vol. 22, no. 18, p. 9987, Sep. 2021, doi: 10.3390/IJMS22189987.

[15] M. Li, X. Chi, Y. Wang, S. Setrerrahmane, W. Xie, and H. Xu, “Trends in insulin resistance: insights into mechanisms and therapeutic strategy,” *Signal Transduction and Targeted Therapy 2022 7:1*, vol. 7, no. 1, pp. 1–25, Jul. 2022, doi: 10.1038/s41392-022-01073-0.

[16] M. Zheng and P. Wang, “Role of insulin receptor substance-1 modulating PI3K/Akt insulin signaling pathway in Alzheimer’s disease,” *3 Biotech 2021 11:4*, vol. 11, no. 4, pp. 1–17, Mar. 2021, doi: 10.1007/S13205-021-02738-3.

[17] J. Miao, Y. Zhang, C. Su, Q. Zheng, and J. Guo, “Insulin-Like Growth Factor Signaling in Alzheimer’s Disease: Pathophysiology and Therapeutic Strategies,” *Molecular Neurobiology 2024 62:3*, vol. 62, no. 3, pp. 3195–3225, Sep. 2024, doi: 10.1007/S12035-024-04457-1.

[18] S. M. De La Monte and J. R. Wands, “Alzheimer’s Disease Is Type 3 Diabetes–Evidence Reviewed,” *Journal of diabetes science and technology (Online)*, vol. 2, no. 6, p. 1101, 2008, doi: 10.1177/193229680800200619.

[19] J. L. Milstein and H. A. Ferris, “The brain as an insulin-sensitive metabolic organ,” *Mol Metab*, vol. 52, p. 101234, Oct. 2021, doi: 10.1016/J.MOLMET.2021.101234.

[20] M. Spinelli, S. Fusco, and C. Grassi, “Brain insulin resistance and hippocampal plasticity: Mechanisms and biomarkers of cognitive decline,” *Front Neurosci*, vol. 10, no. JUL, p. 469184, Jul. 2019, doi: 10.3389/FNINS.2019.00788/XML/NLM.

[21] S. Hoyer, “Is sporadic Alzheimer disease the brain type of non-insulin dependent diabetes mellitus? A challenging hypothesis,” *J Neural Transm*, vol. 105, no. 4–5, pp. 415–422, 1998, doi: 10.1007/S007020050067/METRICS.

[22] S. Hoyer and R. Nitsch, “Cerebral excess release of neurotransmitter amino acids subsequent to reduced cerebral glucose metabolism in early-onset dementia of Alzheimer type,” *J Neural Transm*, vol. 75, no. 3, pp. 227–232, Oct. 1989, doi: 10.1007/BF01258634/METRICS.

[23] A. M. Moloney, R. J. Griffin, S. Timmons, R. O'Connor, R. Ravid, and C. O'Neill, "Defects in IGF-1 receptor, insulin receptor and IRS-1/2 in Alzheimer's disease indicate possible resistance to IGF-1 and insulin signalling," *Neurobiol Aging*, vol. 31, no. 2, pp. 224–243, Feb. 2010, doi: 10.1016/J.NEUROBIOLAGING.2008.04.002.

[24] E. Steen *et al.*, "Impaired insulin and insulin-like growth factor expression and signaling mechanisms in Alzheimer's disease – is this type 3 diabetes?," 2005, Accessed: Apr. 22, 2025. [Online]. Available: https://journals-sagepub-com.zorac.aub.aau.dk/doi/pdf/10.3233/JAD-2005-7107

[25] E. Blázquez, E. Velázquez, V. Hurtado-Carneiro, and J. M. Ruiz-Albusac, "Insulin in the Brain: Its Pathophysiological Implications for States Related with Central Insulin Resistance, Type 2 Diabetes and Alzheimer's Disease," *Front Endocrinol (Lausanne)*, vol. 5, no. OCT, p. 161, 2014, doi: 10.3389/FENDO.2014.00161.

[26] S. M. Gray, R. I. Meijer, and E. J. Barrett, "Insulin Regulates Brain Function, but How Does It Get There?," *Diabetes*, vol. 63, no. 12, p. 3992, Dec. 2014, doi: 10.2337/DB14-0340.

[27] W. Zhao *et al.*, "Brain insulin receptors and spatial memory. Correlated changes in gene expression, tyrosine phosphorylation, and signaling molecules in the hippocampus of water maze trained rats," *Journal of Biological Chemistry*, vol. 274, no. 49, pp. 34893–34902, Dec. 1999, doi: 10.1074/JBC.274.49.34893/ASSET/F9FB2B4F-8B17-4D63-A15E-47E156ABB2C3/MAIN.ASSETS/GR9.JPG.

[28] C. R. Park, R. J. Seeley, S. Craft, and S. C. Woods, "Intracerebroventricular insulin enhances memory in a passive-avoidance task," *Physiol Behav*, vol. 68, no. 4, pp. 509–514, Feb. 2000, doi: 10.1016/S0031-9384(99)00220-6.

[29] A. I. Duarte, P. I. Moreira, and C. R. Oliveira, "Insulin in Central Nervous System: More than Just a Peripheral Hormone," *J Aging Res*, vol. 2012, p. 384017, 2012, doi: 10.1155/2012/384017.

[30] R. U. Margolis and N. Altszuler, "Insulin in the Cerebrospinal Fluid," *Nature 1967 215:5108*, vol. 215, no. 5108, pp. 1375–1376, 1967, doi: 10.1038/2151375a0.

[31] S. C. Woods and D. Porte, "Relationship between plasma and cerebrospinal fluid insulin levels of dogs," *Am J Physiol*, vol. 233, no. 4, 1977, doi: 10.1152/AJPENDO.1977.233.4.E331.

[32] A. Kleinridders, H. A. Ferris, W. Cai, and C. R. Kahn, "Insulin Action in Brain Regulates Systemic Metabolism and Brain Function," *Diabetes*, vol. 63, no. 7, pp. 2232–2243, Jul. 2014, doi: 10.2337/DB14-0568.

[33] W. Chen, W. Cai, B. Hoover, and C. R. Kahn, “Insulin Action in the Brain: Cell Types, Circuits, and Diseases,” *Trends Neurosci*, vol. 45, no. 5, p. 384, May 2022, doi: 10.1016/J.TINS.2022.03.001.

[34] S. H. Lee, J. M. Zabolotny, H. Huang, H. Lee, and Y. B. Kim, “Insulin in the nervous system and the mind: Functions in metabolism, memory, and mood,” *Mol Metab*, vol. 5, no. 8, pp. 589–601, Aug. 2016, doi: 10.1016/J.MOLMET.2016.06.011.

[35] M. Heni, “The insulin resistant brain: impact on whole-body metabolism and body fat distribution,” *Diabetologia 2024 67:7*, vol. 67, no. 7, pp. 1181–1191, Feb. 2024, doi: 10.1007/S00125-024-06104-9.

[36] A. E. Mehran *et al.*, “Hyperinsulinemia Drives Diet-Induced Obesity Independently of Brain Insulin Production,” *Cell Metab*, vol. 16, no. 6, pp. 723–737, Dec. 2012, doi: 10.1016/J.CMET.2012.10.019.

[37] W. S. Young, “Periventricular hypothalamic cells in the rat brain contain insulin mRNA,” *Neuropeptides*, vol. 8, no. 2, pp. 93–97, Aug. 1986, doi: 10.1016/0143-4179(86)90035-1.

[38] D. W. Clarke, L. Mudd, F. T. Boyd, M. Fields, and M. K. Raizada, “Insulin Is Released from Rat Brain Neuronal Cells in Culture,” *J Neurochem*, vol. 47, no. 3, pp. 831–836, Sep. 1986, doi: 10.1111/J.1471-4159.1986.TB00686.X.

[39] T. Kuwabara *et al.*, “Insulin biosynthesis in neuronal progenitors derived from adult hippocampus and the olfactory bulb,” *EMBO Mol Med*, vol. 3, no. 12, p. 742, Dec. 2011, doi: 10.1002/EMMM.201100177.

[40] M. Li, X. Chi, Y. Wang, S. Setrerrahmane, W. Xie, and H. Xu, “Trends in insulin resistance: insights into mechanisms and therapeutic strategy,” *Signal Transduction and Targeted Therapy 2022 7:1*, vol. 7, no. 1, pp. 1–25, Jul. 2022, doi: 10.1038/s41392-022-01073-0.

[41] S. Gabbouj *et al.*, “Altered insulin signaling in Alzheimer’s disease brain-special emphasis on pi3k-akt pathway,” *Front Neurosci*, vol. 13, no. JUN, p. 456800, Jun. 2019, doi: 10.3389/FNINS.2019.00629/BIBTEX.

[42] E. M. Rhea, W. A. Banks, and J. Raber, “Insulin Resistance in Peripheral Tissues and the Brain: A Tale of Two Sites,” *Biomedicines*, vol. 10, no. 7, p. 1582, Jul. 2022, doi: 10.3390/BIOMEDICINES10071582.

[43] G. Scapin *et al.*, “Structure of the insulin receptor–insulin complex by single-particle cryo-EM analysis,” *Nature 2018 556:7699*, vol. 556, no. 7699, pp. 122–125, Feb. 2018, doi: 10.1038/NATURE26153.

[44] E. Choi and X. C. Bai, “The Activation Mechanism of the Insulin Receptor: A Structural Perspective,” *Annu Rev Biochem*, vol. 92, no. Volume 92, 2023, pp. 247–272, Jun. 2023, doi: 10.1146/ANNUREV-BIOCHEM-052521-033250/CITE/REFWORKS.

[45] M. A. Galal *et al.*, “Insulin Receptor Isoforms and Insulin Growth Factor-like Receptors: Implications in Cell Signaling, Carcinogenesis, and Chemoresistance,” *International Journal of Molecular Sciences 2023, Vol. 24, Page 15006*, vol. 24, no. 19, p. 15006, Oct. 2023, doi: 10.3390/IJMS241915006.

[46] A. Belfiore *et al.*, “Insulin Receptor Isoforms in Physiology and Disease: An Updated View,” *Endocr Rev*, vol. 38, no. 5, p. 379, 2017, doi: 10.1210/ER.2017-00073.

[47] N. O. Yunn, J. Kim, S. H. Ryu, and Y. Cho, “A stepwise activation model for the insulin receptor,” *Experimental & Molecular Medicine 2023 55:10*, vol. 55, no. 10, pp. 2147–2161, Oct. 2023, doi: 10.1038/s12276-023-01101-1.

[48] O. Escribano, N. Beneit, C. Rubio-Longás, A. R. López-Pastor, and A. Gómez-Hernández, “The Role of Insulin Receptor Isoforms in Diabetes and Its Metabolic and Vascular Complications,” *J Diabetes Res*, vol. 2017, no. 1, p. 1403206, Jan. 2017, doi: 10.1155/2017/1403206.

[49] I. Camaya, S. Donnelly, and B. O’Brien, “Targeting the PI3K/Akt signaling pathway in pancreatic β-cells to enhance their survival and function: An emerging therapeutic strategy for type 1 diabetes,” *J Diabetes*, vol. 14, no. 4, p. 247, Apr. 2022, doi: 10.1111/1753-0407.13252.

[50] P. D. Leiphrakpam and C. Are, “PI3K/Akt/mTOR Signaling Pathway as a Target for Colorectal Cancer Treatment,” *International Journal of Molecular Sciences 2024, Vol. 25, Page 3178*, vol. 25, no. 6, p. 3178, Mar. 2024, doi: 10.3390/IJMS25063178.

[51] J. Pan *et al.*, “The role of PI3K signaling pathway in Alzheimer’s disease,” *Front Aging Neurosci*, vol. 16, p. 1459025, Sep. 2024, doi: 10.3389/FNAGI.2024.1459025/XML/NLM.

[52] Y. Peng *et al.*, “Scavenging Reactive Oxygen Species Decreases Amyloid-β Levels via Activation of PI3K/Akt/GLUT1 Pathway in N2a/APP695swe Cells,” *Journal of Alzheimer’s Disease*, vol. 90, no. 1, pp. 185–198, 2022, doi: 10.3233/JAD-220610.

[53] N. Guo, X. Wang, M. Xu, J. Bai, H. Yu, and Le Zhang, “PI3K/AKT signaling pathway: Molecular mechanisms and therapeutic potential in depression,” *Pharmacol Res*, vol. 206, p. 107300, Aug. 2024, doi: 10.1016/J.PHRS.2024.107300.

[54] J. Limantoro, B. G. de Liyis, and J. C. Sutedja, “Akt signaling pathway: a potential therapy for Alzheimer’s disease through glycogen synthase kinase 3 beta inhibition,” *The Egyptian Journal of Neurology, Psychiatry and Neurosurgery 2023 59:1*, vol. 59, no. 1, pp. 1–14, Nov. 2023, doi: 10.1186/S41983-023-00751-2.

[55] D. Wang, G. Liu, Y. Meng, H. Chen, Z. Ye, and J. Jing, “The Configuration of GRB2 in Protein Interaction and Signal Transduction,” *Biomolecules 2024, Vol. 14, Page 259*, vol. 14, no. 3, p. 259, Feb. 2024, doi: 10.3390/BIOM14030259.

[56] M. Leclerc *et al.*, “Cerebrovascular insulin receptors are defective in Alzheimer’s disease,” *Brain*, vol. 146, no. 1, p. 75, Jan. 2022, doi: 10.1093/BRAIN/AWAC309.

[57] N. Beneit *et al.*, “Expression of insulin receptor (IR) A and B isoforms, IGF-IR, and IR/IGF-IR hybrid receptors in vascular smooth muscle cells and their role in cell migration in atherosclerosis,” *Cardiovasc Diabetol*, vol. 15, no. 1, pp. 1–14, Dec. 2016, doi: 10.1186/S12933-016-0477-3/FIGURES/7.

[58] E. Osher and V. M. Macaulay, “Therapeutic targeting of the IGF axis,” *Cells*, vol. 8, no. 8, Aug. 2019, doi: 10.3390/CELLS8080895.

[59] A. Arjunan, D. K. Sah, M. Woo, and J. Song, “Identification of the molecular mechanism of insulin-like growth factor-1 (IGF-1): a promising therapeutic target for neurodegenerative diseases associated with metabolic syndrome,” *Cell & Bioscience 2023 13:1*, vol. 13, no. 1, pp. 1–18, Jan. 2023, doi: 10.1186/S13578-023-00966-Z.

[60] C. Talia, L. Connolly, and P. A. Fowler, “The insulin-like growth factor system: A target for endocrine disruptors?,” *Environ Int*, vol. 147, p. 106311, Feb. 2021, doi: 10.1016/J.ENVINT.2020.106311.

[61] S. J. Turvey, M. J. McPhillie, M. T. Kearney, S. P. Muench, K. J. Simmons, and C. W. G. Fishwick, “Recent developments in the structural characterisation of the IR and IGF1R: implications for the design of IR–IGF1R hybrid receptor modulators,” *RSC Med Chem*, vol. 13, no. 4, p. 360, Feb. 2022, doi: 10.1039/D1MD00300C.

[62] A. J. Blyth, N. S. Kirk, and B. E. Forbes, “Understanding IGF-II Action through Insights into Receptor Binding and Activation,” *Cells*, vol. 9, no. 10, Oct. 2020, doi: 10.3390/CELLS9102276.

[63] D. N. Boone and A. V. Lee, “Targeting the Insulin-like Growth Factor Receptor: Developing Biomarkers from Gene Expression Profiling,” *Crit Rev Oncog*, vol. 17, no. 2, p. 161, 2012, doi: 10.1615/CRITREVONCOG.V17.I2.30.

[64] M. Andersen, D. Nørgaard-Pedersen, J. Brandt, I. Pettersson, and R. Slaaby, “IGF1 and IGF2 specificities to the two insulin receptor isoforms are determined by insulin receptor amino acid 718,” *PLoS One*, vol. 12, no. 6, p. e0178885, Jun. 2017, doi: 10.1371/JOURNAL.PONE.0178885.

[65] J. S. Lee, C. E. Tocheny, and L. M. Shaw, “The Insulin-like Growth Factor Signaling Pathway in Breast Cancer: An Elusive Therapeutic Target,” *Life 2022, Vol. 12, Page 1992*, vol. 12, no. 12, p. 1992, Nov. 2022, doi: 10.3390/LIFE12121992.

[66] Z. Cao, J. Min, Q. Tan, K. Si, H. Yang, and C. Xu, “Circulating insulin-like growth factor-1 and brain health: Evidence from 369,711 participants in the UK Biobank,” *Alzheimers Res Ther*, vol. 15, no. 1, pp. 1–10, Dec. 2023, doi: 10.1186/S13195-023-01288-5/FIGURES/2.

[67] P. S. Van Dam and A. Aleman, “Insulin-like growth factor-I, cognition and brain aging,” *Eur J Pharmacol*, vol. 490, no. 1–3, pp. 87–95, Apr. 2004, doi: 10.1016/J.EJPHAR.2004.02.047.

[68] W. Westwoo *et al.*, “Insulin-like growth factor-1 and risk of Alzheimer dementia and brain atrophy,” *Neurology*, vol. 82, no. 18, p. 1613, May 2014, doi: 10.1212/WNL.0000000000000382.

[69] S. Al-Samerria and S. Radovick, “The Role of Insulin-like Growth Factor-1 (IGF-1) in the Control of Neuroendocrine Regulation of Growth,” *Cells*, vol. 10, no. 10, p. 2664, Oct. 2021, doi: 10.3390/CELLS10102664.

[70] W. Alata *et al.*, “Targeting insulin-like growth factor-1 receptor (IGF1R) for brain delivery of biologics,” *The FASEB Journal*, vol. 36, no. 3, p. e22208, Mar. 2022, doi: 10.1096/FJ.202101644R.

[71] M. C. Selles *et al.*, “Adenovirus-mediated transduction of insulin-like growth factor 1 protects hippocampal neurons from the toxicity of Aβ oligomers and prevents memory loss in an Alzheimer mouse model,” *Mol Neurobiol*, vol. 57, no. 3, p. 1473, Mar. 2019, doi: 10.1007/S12035-019-01827-Y.

[72] L. K. Bale, S. A. West, N. M. Gades, D. J. Baker, and C. A. Conover, “Gene deletion of Pregnancy-associated Plasma Protein-A (PAPP-A) improves pathology and cognition in an Alzheimer’s disease mouse model,” *Exp Neurol*, vol. 382, p. 114976, Dec. 2024, doi: 10.1016/J.EXPNEUROL.2024.114976.

[73] E. Cohen *et al.*, “Reduced IGF-1 Signaling Delays Age-Associated Proteotoxicity in Mice,” *Cell*, vol. 139, no. 6, pp. 1157–1169, Dec. 2009, doi: 10.1016/J.CELL.2009.11.014.

[74] S. Freude *et al.*, “Neuronal IGF-1 resistance reduces Aβ accumulation and protects against premature death in a model of Alzheimer’s disease,” *The FASEB Journal*, vol. 23, no. 10, pp. 3315–3324, Oct. 2009, doi: 10.1096/FJ.09-132043.

[75] R. Slaaby, “Specific insulin/IGF1 hybrid receptor activation assay reveals IGF1 as a more potent ligand than insulin,” *Scientific Reports 2015 5:1*, vol. 5, no. 1, pp. 1–5, Jan. 2015, doi: 10.1038/srep07911.

[76] R. Slaaby, “Specific insulin/IGF1 hybrid receptor activation assay reveals IGF1 as a more potent ligand than insulin,” *Scientific Reports 2015 5:1*, vol. 5, no. 1, pp. 1–5, Jan. 2015, doi: 10.1038/srep07911.

[77] X. Li *et al.*, "A brain-derived insulin signal encodes protein satiety for nutrient-specific feeding inhibition," *Cell Rep*, vol. 43, no. 6, p. 114282, Jun. 2024, doi: 10.1016/J.CELREP.2024.114282.

[78] J. Chen, A. M. Nagle, Y. F. Wang, D. N. Boone, and A. V. Lee, "Controlled dimerization of insulin-like growth factor-1 and insulin receptors reveals shared and distinct activities of holo and hybrid receptors," *J Biol Chem*, vol. 293, no. 10, p. 3700, Mar. 2018, doi: 10.1074/JBC.M117.789503.

[79] A. M. Fernández *et al.*, "Functional inactivation of the IGF-I and insulin receptors in skeletal muscle causes type 2 diabetes," *Genes Dev*, vol. 15, no. 15, p. 1926, Aug. 2001, doi: 10.1101/GAD.908001.

[80] N. A. Tan, A. M. A. Carpio, H. C. Heller, and E. C. Pittaras, "Behavioral and Neuronal Characterizations, across Ages, of the TgSwDI Mouse Model of Alzheimer's Disease," *Genes 2024, Vol. 15, Page 47*, vol. 15, no. 1, p. 47, Dec. 2023, doi: 10.3390/GENES15010047.

[81] G. D. Van Vickle *et al.*, "Tg-SwDI Transgenic Mice Exhibit Novel Alterations in AβPP Processing, Aβ Degradation, and Resilient Amyloid Angiopathy," *Am J Pathol*, vol. 173, no. 2, p. 483, 2008, doi: 10.2353/AJPATH.2008.071191.

[82] J. Davis *et al.*, "Early-onset and Robust Cerebral Microvascular Accumulation of Amyloid β-Protein in Transgenic Mice Expressing Low Levels of a Vasculotropic Dutch/Iowa Mutant Form of Amyloid β-Protein Precursor," *Journal of Biological Chemistry*, vol. 279, no. 19, pp. 20296–20306, May 2004, doi: 10.1074/JBC.M312946200.

[83] S. B. Al Rihani, R. S. Lan, A. Kaddoumi, and F. Gosselet, "Granisetron Alleviates Alzheimer's Disease Pathology in TgSwDI Mice Through Calmodulin-Dependent Protein Kinase II/cAMP-Response Element Binding Protein Pathway," *Journal of Alzheimer's Disease*, vol. 72, no. 4, pp. 1097–1117, 2019, doi: 10.3233/JAD-190849/SUPPL_FILE/SJ-DOCX-1-ALZ-10.3233_JAD-190849.DOCX.

[84] T. Moos and E. H. Morgan, "The significance of the mutated divalent metal transporter (DMT1) on iron transport into the Belgrade rat brain," *J Neurochem*, vol. 88, no. 1, pp. 233–245, Jan. 2004, doi: 10.1046/J.1471-4159.2003.02142.X.

[85] "Human Insulin R/CD220 Antibody AF1544: R&D Systems." Accessed: May 27, 2025. [Online]. Available: https://www.rndsystems.com/products/human-insulin-r-cd220-antibody_af1544

[86] S. Cruz Biotechnology, "IGF-IRα (2C8): sc-463", Accessed: May 27, 2025. [Online]. Available: www.scbt.com

[87] “Phospho-IGF-I Receptor β (Tyr1131)/Insulin Receptor β (Tyr1146) Antibody | Cell Signaling Technology.” Accessed: May 27, 2025. [Online]. Available: https://www.cellsignal.com/products/primary-antibodies/phospho-igf-i-receptor-b-tyr1131-insulin-receptor-b-tyr1146-antibody/3021?srsltid=AfmBOoqvEC0LrgX5NbBQCEqk62Xi2oybYy01frg_vTbfVIrzYZHRhiH9

[88] “HRP-Donkey Anti-Goat IgG (H+L) (min X) Secondary Antibody | JIR.” Accessed: May 27, 2025. [Online]. Available: https://www.jacksonimmuno.com/catalog/products/705-035-147

[89] “goat anti-rabbit IgG-HRP: sc-2004,” SANTA CRUZ BIOTECHNOLOGY, INC. Accessed: May 27, 2025. [Online]. Available: https://datasheets.scbt.com/sc-2004.pdf

[90] Y. Lee *et al.*, “Hyperglycemia in rodent models of type 2 diabetes requires insulin-resistant alpha cells,” *Proc Natl Acad Sci U S A*, vol. 111, no. 36, pp. 13217–13222, Sep. 2014, doi: 10.1073/PNAS.1409638111/SUPPL_FILE/PNAS.201409638SI.PDF.

[91] S. H. Lee, H. J. Park, H. K. Chun, S. Y. Cho, S. M. Cho, and H. S. Lillehoj, “Dietary phytic acid lowers the blood glucose level in diabetic KK mice,” *Nutrition Research*, vol. 26, no. 9, pp. 474–479, Sep. 2006, doi: 10.1016/J.NUTRES.2006.06.017.

[92] L. Pillai-Kastoori, A. R. Schutz-Geschwender, and J. A. Harford, “A systematic approach to quantitative Western blot analysis,” *Anal Biochem*, vol. 593, p. 113608, Mar. 2020, doi: 10.1016/J.AB.2020.113608.

[93] “Revert Total Protein Stain for Accurate Western Normalization.” Accessed: May 27, 2025. [Online]. Available: https://shop.licor.com/bio/reagents/revert-total-protein-stain-for-western-blot-normalization

[94] “Determining the Linear Range for Quantitative Western Blot Detection.” Accessed: May 27, 2025. [Online]. Available: https://www.licorbio.com/support/contents/applications/western-blots/western-blot-linear-range-determination.html

[95] “Finding the Combined Linear Range with Empiria Studio.” Accessed: May 27, 2025. [Online]. Available: https://bio.licor.com/bio/help/empiria_studio/software/empiria_studio/calculate/blot/linear-range-determination.html

[96] “Chemiluminescent Western Blotting | Thermo Fisher Scientific - DK.” Accessed: May 27, 2025. [Online]. Available: https://www.thermofisher.com/dk/en/home/life-science/protein-biology/protein-biology-learning-center/protein-biology-resource-library/pierce-protein-methods/chemiluminescent-western-blotting.html

[97] “Western Blot Troubleshooting | Thermo Fisher Scientific - DK.” Accessed: May 27, 2025. [Online]. Available: https://www.thermofisher.com/dk/en/home/life-science/protein-biology/protein-biology-learning-center/protein-gel-electrophoresis-information/western-blot-troubleshooting.html

[98] “Western Blot Doctor™ — Protein Band Size and Pattern Problems | Bio-Rad.” Accessed: May 27, 2025. [Online]. Available: https://www.bio-rad.com/en-dk/applications-technologies/western-blot-doctor-protein-band-size-pattern-problems?ID=MIW4MCKG4

[99] X. Yan, E. Managlia, Y. Y. Zhao, X. Di Tan, and I. G. De Plaen, “Macrophage-derived IGF-1 protects the neonatal intestine against necrotizing enterocolitis by promoting microvascular development,” *Commun Biol*, vol. 5, no. 1, p. 320, Dec. 2022, doi: 10.1038/S42003-022-03252-9.

[100] M. Rodríguez *et al.*, “Central Downregulation of S-Resistin Alleviates Inflammation in EWAT and Liver and Prevents Adipocyte Hypertrophy,” *J Endocr Soc*, vol. 9, no. 2, p. bvae224, Feb. 2025, doi: 10.1210/JENDSO/BVAE224.

[101] M. Hersom, H. C. Helms, C. Schmalz, T. Pedersen, S. T. Buckley, and B. Brodin, “The insulin receptor is expressed and functional in cultured blood-brain barrier endothelial cells but does not mediate insulin entry from blood to brain,” *Am J Physiol Endocrinol Metab*, vol. 315, no. 4, pp. E531–E542, Oct. 2018, doi: 10.1152/AJPENDO.00350.2016/ASSET/IMAGES/LARGE/ZH10051878950007.JPEG.

[102] “Single Cell RNA-seq Gene Expression Data.” Accessed: May 27, 2025. [Online]. Available: http://betsholtzlab.org/VascularSingleCells/database.html?gene=INSR

[103] M. Vanlandewijck *et al.*, “A molecular atlas of cell types and zonation in the brain vasculature,” *Nature 2018 554:7693*, vol. 554, no. 7693, pp. 475–480, Feb. 2018, doi: 10.1038/nature25739.

[104] L. He *et al.*, “Single-cell RNA sequencing of mouse brain and lung vascular and vessel-associated cell types,” *Scientific Data 2018 5:1*, vol. 5, no. 1, pp. 1–11, Aug. 2018, doi: 10.1038/sdata.2018.160.

[105] E. M. Ribe and S. Lovestone, “Insulin signalling in Alzheimer's disease and diabetes: from epidemiology to molecular links,” *J Intern Med*, vol. 280, no. 5, pp. 430–442, Nov. 2016, doi: 10.1111/JOIM.12534.

[106] Y. Liu, F. Liu, I. Grundke-Iqbal, K. Iqbal, and C. X. Gong, “Deficient brain insulin signalling pathway in Alzheimer’s disease and diabetes,” *J Pathol*, vol. 225, no. 1, p. 54, Sep. 2011, doi: 10.1002/PATH.2912.

[107] C. M. Griffith *et al.*, “Impaired Glucose Tolerance and Reduced Plasma Insulin Precede Decreased AKT Phosphorylation and GLUT3 Translocation in the Hippocampus of Old 3xTg-AD Mice,” *Journal of Alzheimer’s Disease*, vol. 68, no. 2, pp. 809–837, 2019, doi: 10.3233/JAD-180707.

[108] Y. Chen *et al.*, “Intranasal insulin restores insulin signaling, increases synaptic proteins, and reduces Aβ level and microglia activation in the brains of 3xTg-AD mice,” *Exp Neurol*, vol. 261, pp. 610–619, 2014, doi: 10.1016/J.EXPNEUROL.2014.06.004.

[109] W. Zhang *et al.*, “Differential expression of receptors mediating receptor-mediated transcytosis (RMT) in brain microvessels, brain parenchyma and peripheral tissues of the mouse and the human,” *Fluids Barriers CNS*, vol. 17, no. 1, p. 47, Jul. 2020, doi: 10.1186/S12987-020-00209-0.

[110] O. Escribano, C. Guillén, C. Nevado, A. Gomez-Hernández, C. R. Kahn, and M. Benito, “β-Cell Hyperplasia Induced by Hepatic Insulin Resistance: Role of a Liver-Pancreas Endocrine Axis Through Insulin Receptor A Isoform,” *Diabetes*, vol. 58, no. 4, p. 820, Apr. 2009, doi: 10.2337/DB08-0551.

[111] M. T. Traversy *et al.*, “Altered cerebral insulin response in transgenic mice expressing the epsilon-4 allele of the human apolipoprotein E gene,” *Psychoneuroendocrinology*, vol. 77, p. 203, Mar. 2016, doi: 10.1016/J.PSYNEUEN.2016.11.028.

[112] C. B. Haas *et al.*, “Brain Insulin Administration Triggers Distinct Cognitive and Neurotrophic Responses in Young and Aged Rats,” *Mol Neurobiol*, vol. 53, no. 9, pp. 5807–5817, Nov. 2016, doi: 10.1007/S12035-015-9494-6/FIGURES/6.

[113] C. A. Grillo, G. G. Piroli, R. M. Hendry, and L. P. Reagan, “INSULIN-STIMULATED TRANSLOCATION OF GLUT4 TO THE PLASMA MEMBRANE IN RAT HIPPOCAMPUS IS PI3-KINASE DEPENDENT,” *Brain Res*, vol. 1296, p. 35, Oct. 2009, doi: 10.1016/J.BRAINRES.2009.08.005.

[114] M. Sajan *et al.*, “Brain insulin signaling is increased in insulin-resistant states and decreases in FOXOs and PGC-1a and increases in Aβ1-40/42 and phospho-tau may abet Alzheimer development,” *Diabetes*, vol. 65, no. 7, pp. 1892–1903, Jul. 2016, doi: 10.2337/DB15-1428/-/DC1.

[115] B. Clodfelder-Miller, P. De Sarno, A. A. Zmijewska, L. Song, and R. S. Jope, “Physiological and Pathological Changes in Glucose Regulate Brain Akt and Glycogen Synthase Kinase-3,” *J Biol Chem*, vol. 280, no. 48, p. 39723, Dec. 2005, doi: 10.1074/JBC.M508824200.

[116] Y. Jiang *et al.*, “Effect of Peripheral Insulin Administration on Phosphorylation of Tau in the Brain,” *Journal of Alzheimer’s Disease*, vol. 75, no. 4, pp. 1169–1180, May 2020, doi:

10.3233/JAD-200147/ASSET/58F084AE-3ECF-4098-9CA7-C953AE523175/ASSETS/GRAPHIC/10.3233_JAD-200147-FIG7.JPG.

[117] T. Sartorius *et al.*, “The Brain Response to Peripheral Insulin Declines with Age: A Contribution of the Blood-Brain Barrier?,” *PLoS One*, vol. 10, no. 5, p. e0126804, May 2015, doi: 10.1371/JOURNAL.PONE.0126804.

[118] M. Vandal *et al.*, “Insulin Reverses the High-Fat Diet–Induced Increase in Brain Aβ and Improves Memory in an Animal Model of Alzheimer Disease,” *Diabetes*, vol. 63, no. 12, pp. 4291–4301, Dec. 2014, doi: 10.2337/DB14-0375.

[119] S. Freude *et al.*, “Peripheral Hyperinsulinemia Promotes Tau Phosphorylation In Vivo,” *Diabetes*, vol. 54, no. 12, pp. 3343–3348, Dec. 2005, doi: 10.2337/DIABETES.54.12.3343.

[120] A. P. Muller *et al.*, “Exercise increases insulin signaling in the hippocampus: Physiological effects and pharmacological impact of intracerebroventricular insulin administration in mice,” *Hippocampus*, vol. 21, no. 10, pp. 1082–1092, Oct. 2011, doi: 10.1002/HIPO.20822.

Appendices

A.1 WBs of INSRα Isoforms

A.1.1 TgSwDI mice (18 months)

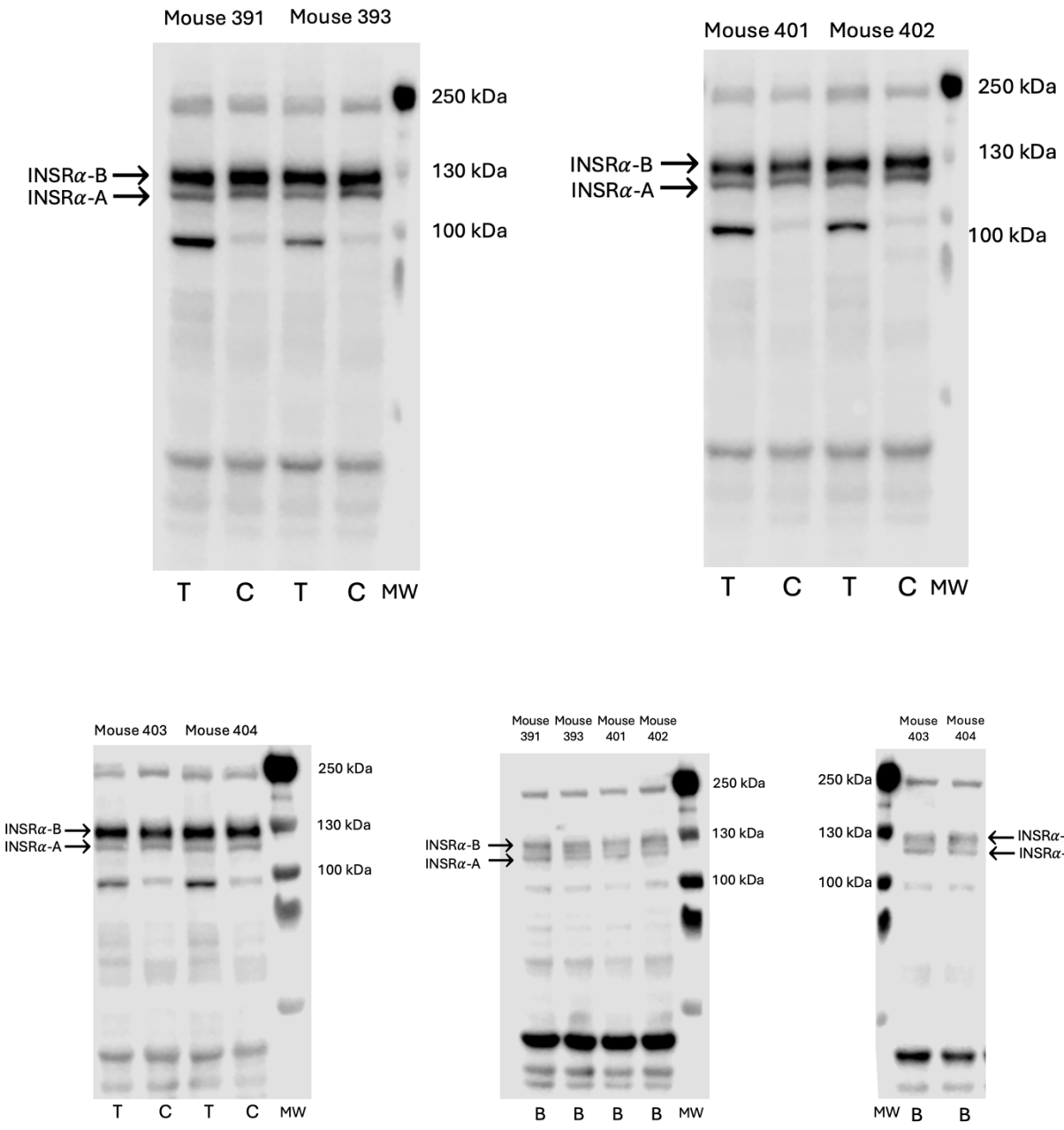

T: Total brain, C: capillaries, B: Brain fraction, MW: Molecular weight

A.1.2 TgSwDI mice (30 months)

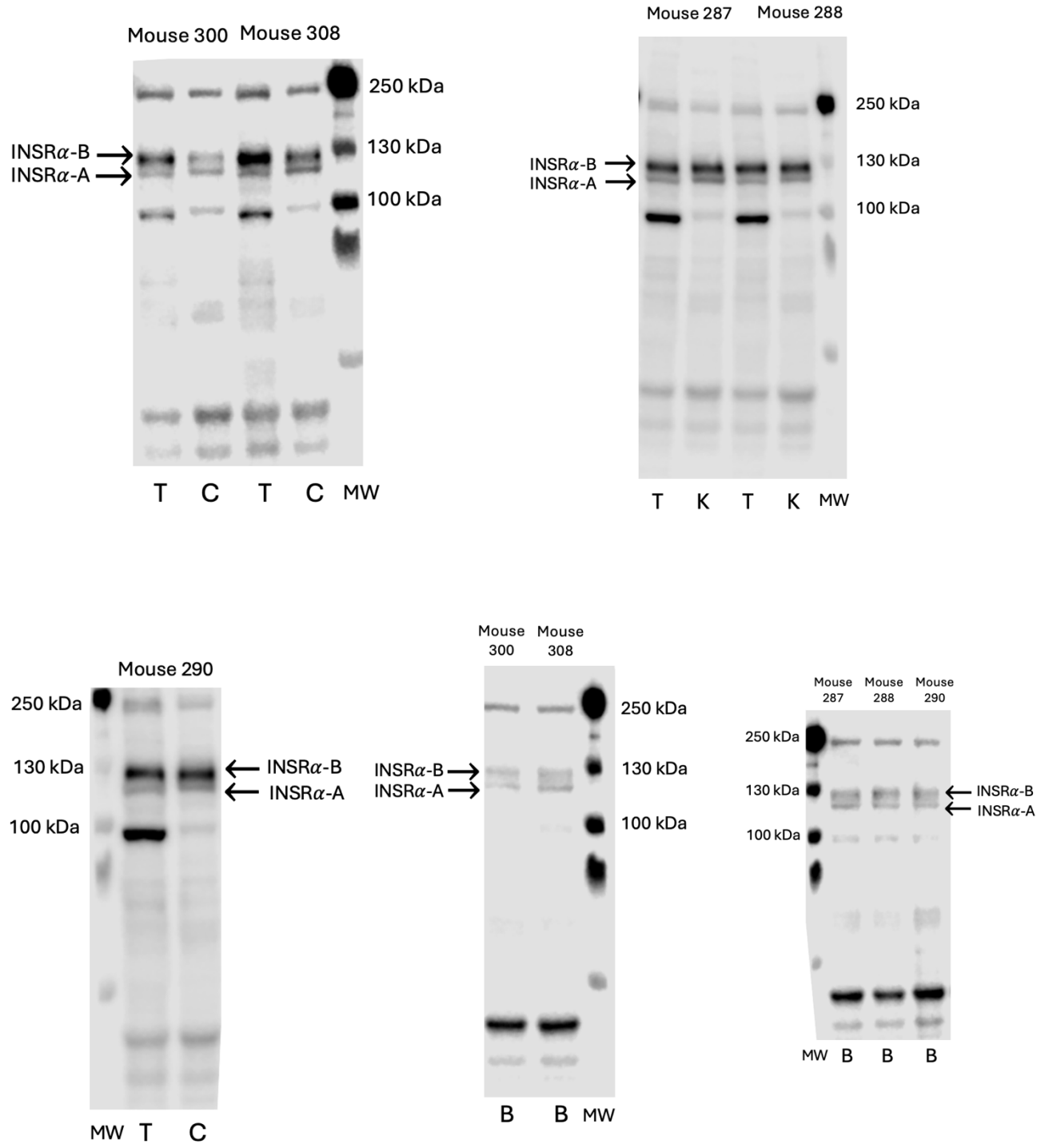

T: Total brain, C: Capillaries, B: Brain fraction, MW: Molecular weight

A.1.3 WT mice (12 months)

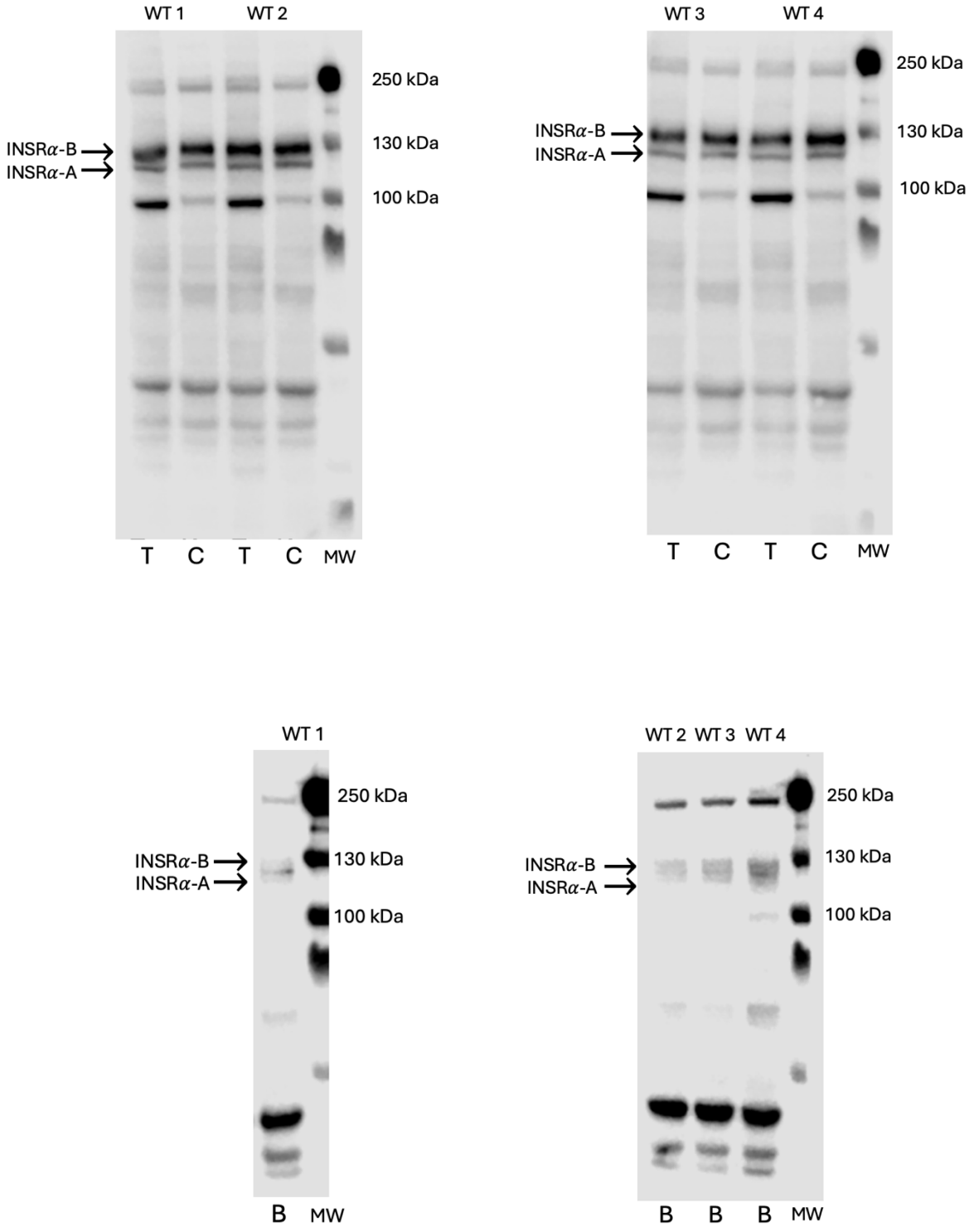

T: Total brain, C: Capillaries, B: Brain fraction, MW: Molecular weight, WT: Wild-type

A.2 WBs of IGF-1R

A.2.1 TgSwDI mice (18 months)

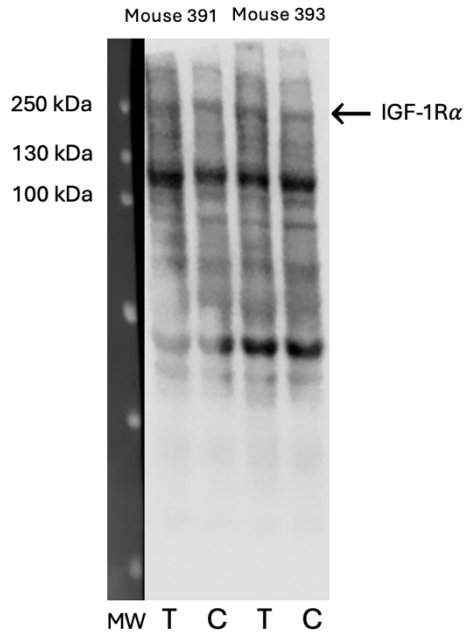

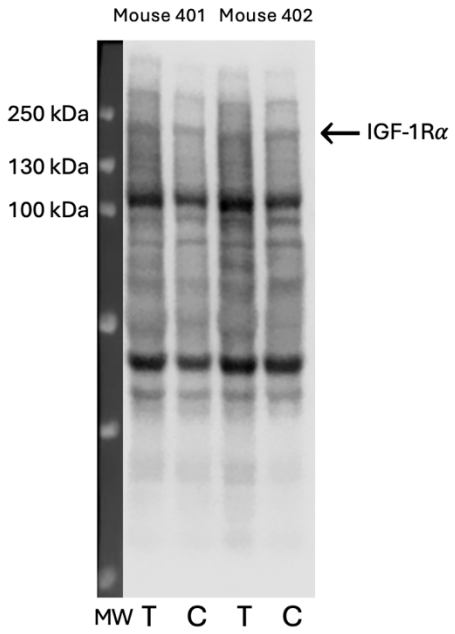

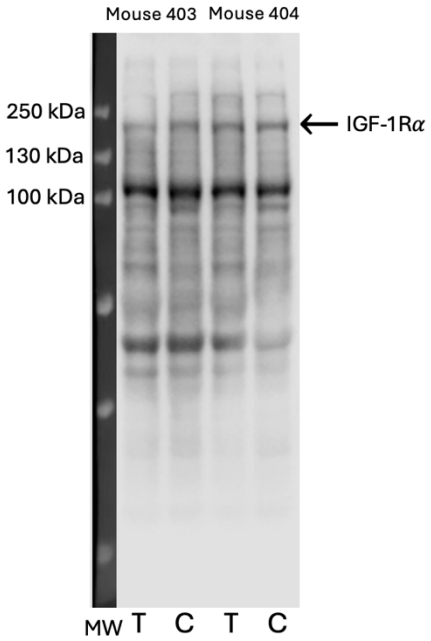

T: Total brain, C: Capillaries, MW: Molecular weight

A.2.2 TgSwDI mice (30 months)

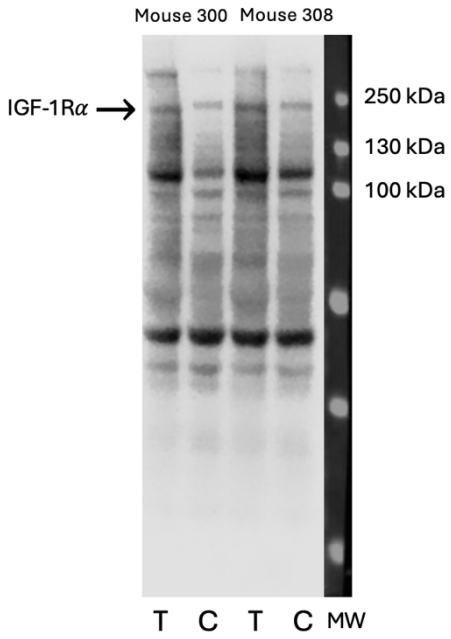

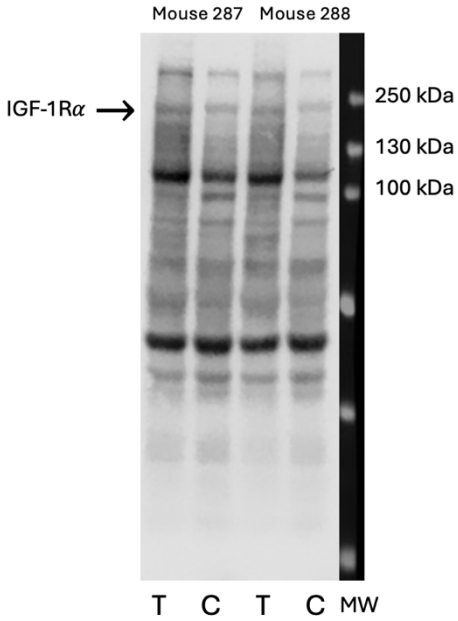

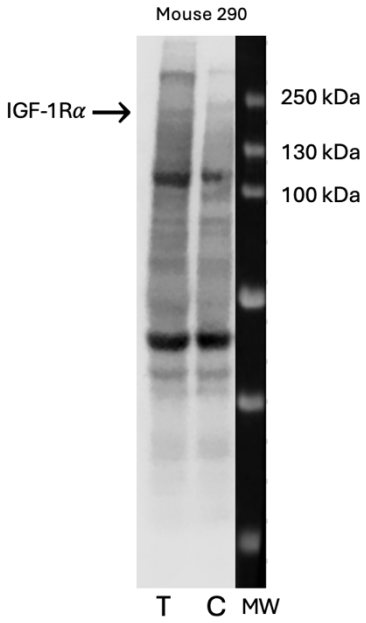

T: Total brain, C: Capillaries, MW: Molecular weight

A.2.3 WT mice (12 months)

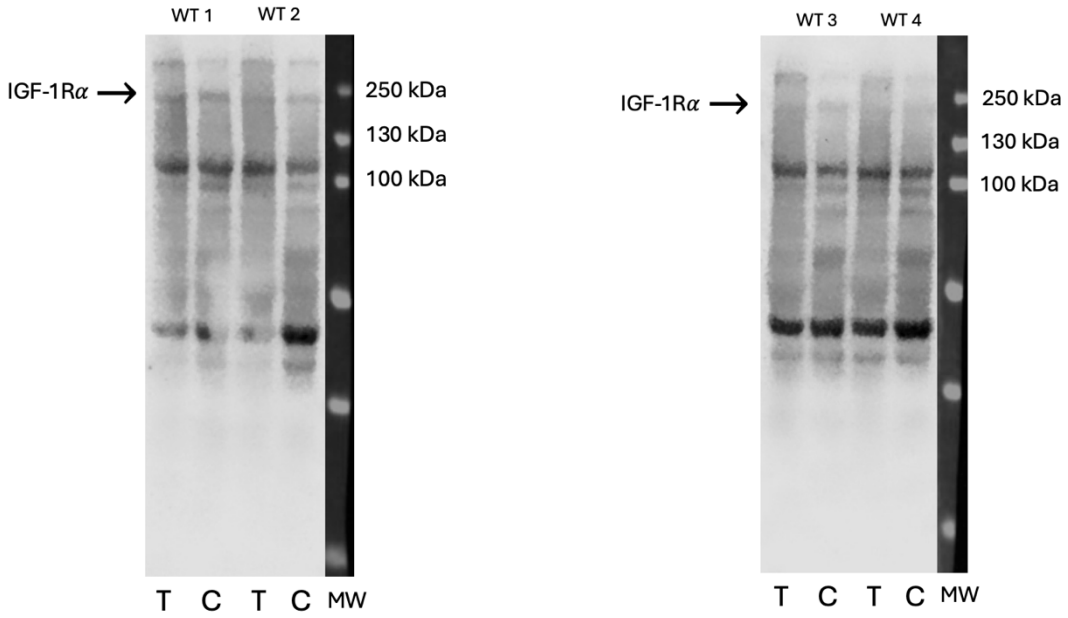

T: Total brain, C: Capillaries, MW: Molecular weight, WT: Wild-type

A.3 WBs of pIGF-1Rβ/INSRβ

A.3.1 TgSwDI mice (15 months) - insulin injection

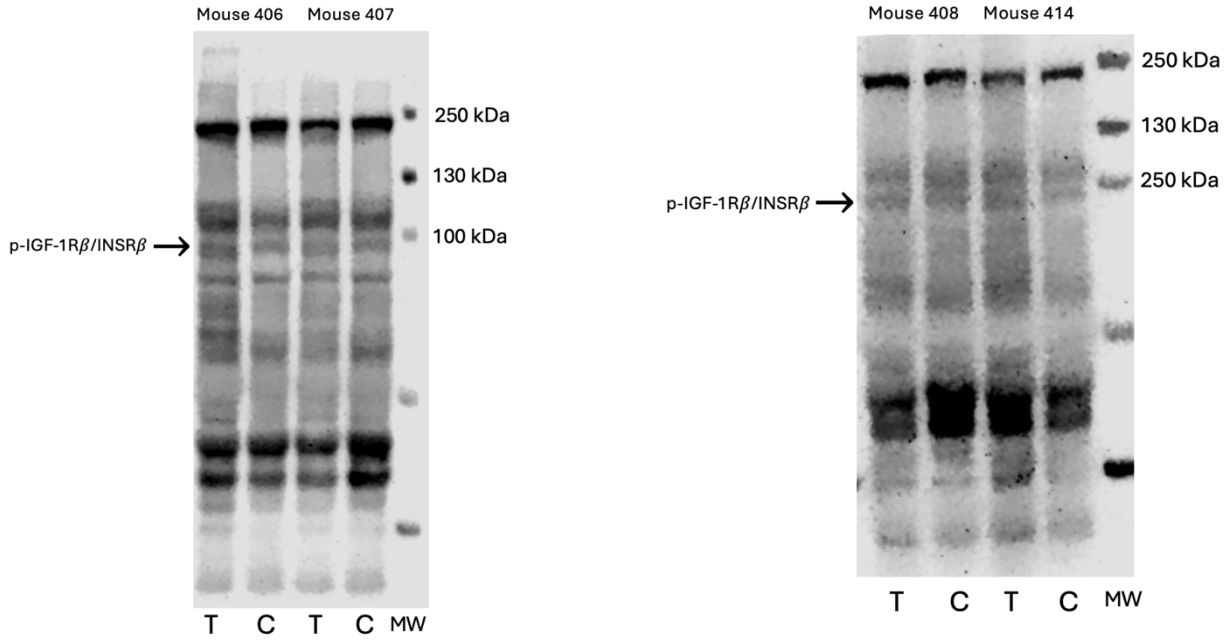

T: Total brain, C: Capillaries, MW: Molecular weight

A.3.2 TgSwDI mice (15 months) - saline injection

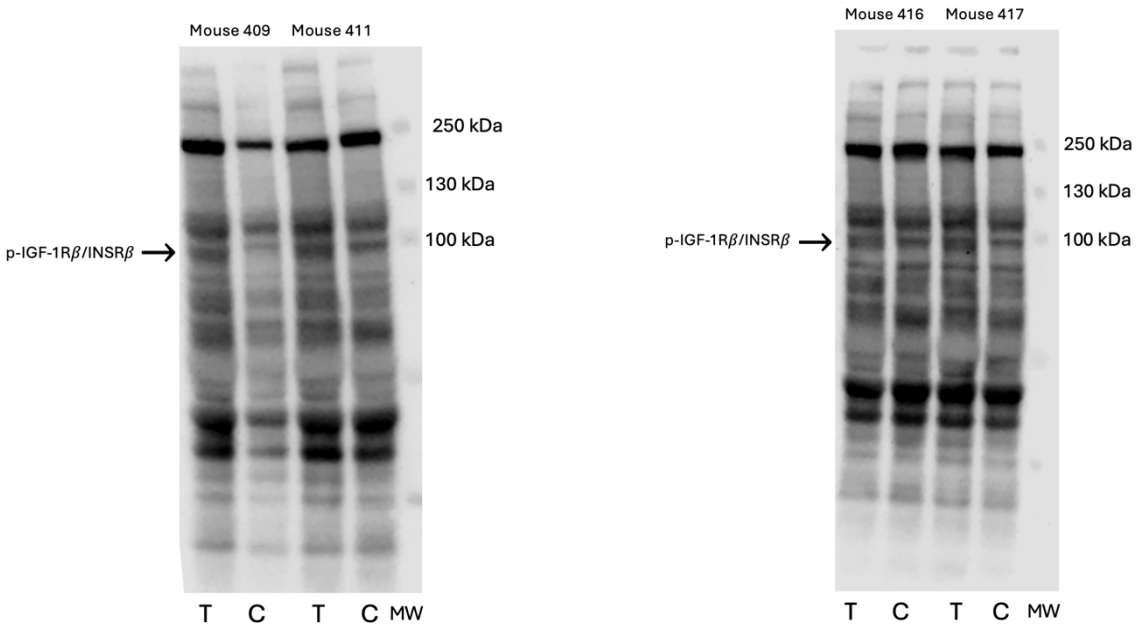

T: Total brain, C: Capillaries, MW: Molecular weight

A.3.3 WT mice (12 months) - insulin injection

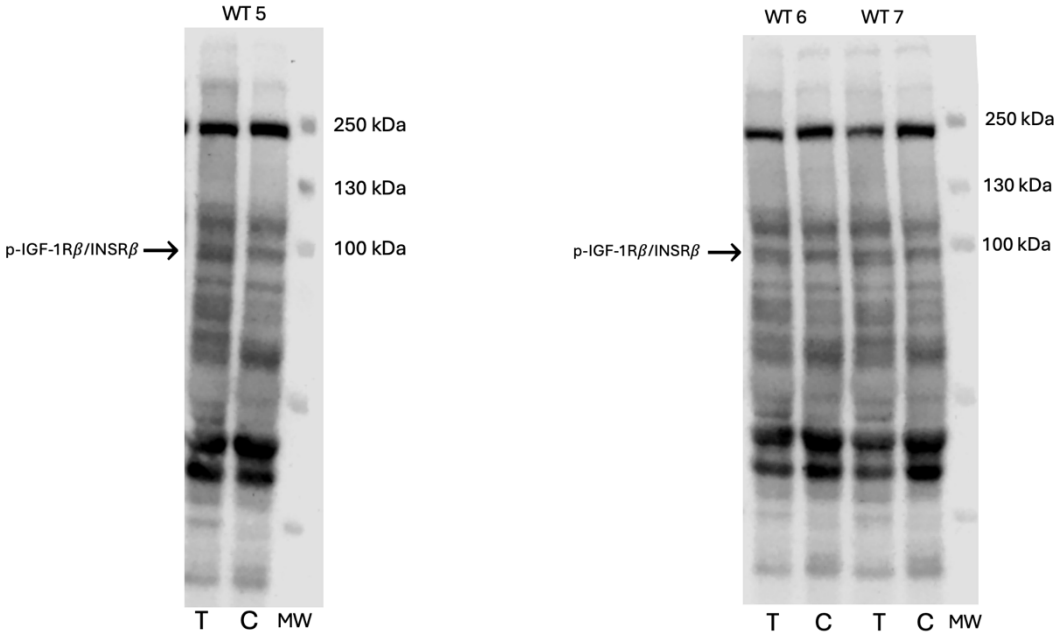

T: Total brain, C: Capillaries, MW: Molecular weight, WT: Wild-type

A.3.4 WT mice (12 months) - saline injection

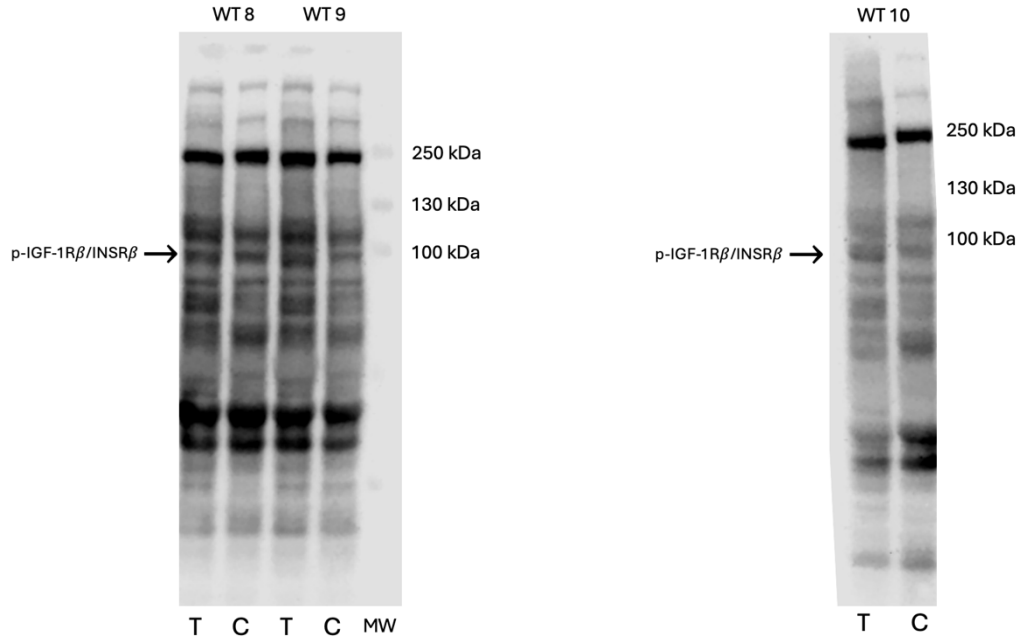

T: Total brain, C: Capillaries, MW: Molecular weight, WT: Wild-type

Use of Artificial-Intelligence (AI) Generated Content

As a student in the MedIS program at AAU, it's important to be aware of how you may and may not use generative AI, such as ChatGPT/Microsoft Copilot, in connection with your studies.

If you choose to utilize AI for your projects, it's crucial to apply the technology in accordance with good scientific practice, including data protection regulations (GDPR). While AI can enhance readability and language, it has several limitations related to validity, bias, quality, and reliability that challenge two fundamental principles of research integrity: accountability and honesty. Always review and edit the suggestions provided by AI carefully.

Be especially cautious if you have used or plan to use generative AI on your own materials, such as images or other types of data, as this could raise suspicions of forgery or manipulation. In your report, include a declaration stating if you have used AI, specify the purpose, and provide details about the AI system used.

Examples of advantages and risks of using AI:

Purpose	Can AI help	Advantages and Risk
Formulate a research question	Yes	**A:** as a virtual conversation partner for idea generation **R:** the argumentation may not be correct and scientifically sound
Literature search	To some degree	**A:** it may be an idea to ask the AI for an overview to check for possible non-peer review articles/grey literature **R:** AI can invent non-existing references. It is important to critically check all suggestions. In your project, you must always carry out a correct literature search with a search string that can be verified
Critical literature assessment	No	**A:** - **R:** AI can reference a debate about the quality of an article but not perform a quality analysis/assessment
Synthesize literature	Yes	**A:** AI can make small, condensed abstracts of an article **R:** Important information can be lost, and data can be misinterpreted if you do not know what the articles contain
Generated/manipulated code	Yes	**A:** fast **R:** overeager to generate an output. You must always ensure that the code performs as desired
Generated/manipulated image	No	**A:** - **R:** could ruin the validity and induce forgery or manipulation
Data analysis	No	**A:** - **R:** data to be considered published when they are entered into AI, and with that, the news value/property right disappears.

Writing article/report	To some degree	**A:** you can use AI as inspiration to formulate paragraphs. In addition, it can help as a spell checker and grammar checker, but it is not perfect. **R:** if you put the entire report/article into AI, it will be considered published, and in principle, it will be a matter of plagiarism when you upload it to a digital exam
Create presentations	To some degree	**A:** AI can generate design suggestions so that your slides have a professional look **R:** There is no access to Copilot in PP at AAU (May 2024)
Communicate to laymen/non-specialists	Yes	**A:** AI can rewrite a text targeted at a specific target group and LIX number **R:** It is important to critically check all suggestions.

At AAU we use Copilot; Copilot - Aalborg University (aau.dk). Remember to **use your AAU account when logging into Copilot**, which ensures you are in a secure environment. This is indicated by the word 'Protected' or 'Beskyttet' on a green background. It means that you are in a closed prompt, where responses are not saved or used to train the model, thereby eliminating the risk of leaking information outside AAU.

Disclosure – Use of Artificial-Intelligence (AI) Generated Content

Students must acknowledge all use of AI

Select all applicable statements and complete the text if applicable.

1. Disclosure: No AI use

☐ I acknowledge that no AI tools/technologies (Grammarly, ChatGPT, Bard, Quillbot, OpenAI etc.) were used in the completion of this assessment.

2. Disclosure: Formulate research question

(X) I acknowledge the use of ChatGPT to formulate some research questions to get inspired and obtain ideas.

Eksempler kan være:

1. Jeg vil gerne undersøge om man kan påvise hjerne insulin resistens i hjernens blodkar ved eksperimentel Alzheimers. Har du ideer til, hvilke forsøg jeg kan lave? Jeg kan gøre brug af AD mus.
2. Kan du give ideer til, hvad man kan fokusere på, hvis man gerne vil fastslå hvad præcis definering af hjerne insulin resistens kan medføre i fremtiden?

3. Disclosure: Literature search

☐ I acknowledge the use of XYZ, version, Month, Year (web URL) to search for literature. I entered the following prompts on Date, Month, Year:

Original prompt: "Paste the prompt"

Follow-up prompt: "Paste the prompt"

The output from these prompts was used to state what action was made using the output.

4. Disclosure: Critical literature assessment

☐ I acknowledge the use of XYZ, version, Month, Year (web URL) to assess my literature. I entered the following prompts on Date, Month, Year:

Original prompt: "Paste the prompt"

Follow-up prompt: "Paste the prompt"

The output from these prompts was used to state what action was made using the output.

5. Disclosure: Synthesize literature

☐ I acknowledge the use of XYZ, version, Month, Year (web URL) to synthesize the literature. I entered the following prompts on Date, Month, Year:

Original prompt: "Paste the prompt"

Follow-up prompt: "Paste the prompt"

The output from these prompts was used to state what action was made using the output.

6. Disclosure: Generated/manipulated code – list each occurrence

☐ I acknowledge the use of XYZ, version, Month, Year (web URL) to explain what you used AI for. I entered the following prompt on Date, Month, Year:

"Paste the prompt"

The output from these prompts was used to explain what the code was used for.

7. Disclosure: Generated/manipulated image – list each occurrence

☐ I acknowledge the use of XYZ, version, Month, Year (web URL) to explain what you used AI for. I entered the following prompt on Date, Month, Year:

"Paste the prompt"

The output from these prompts was used to explain what the image was used for.

8. Disclosure: Data analysis

☐ I acknowledge the use of XYZ, version, Month, Year (web URL) to analyze data. I entered the following prompts on Date, Month, Year:

Original prompt: "Paste the prompt"

Follow-up prompt: "Paste the prompt"

The output from these prompts was used to state what action was made using the output.

9. Disclosure: Generate or rephrase text incl. edit/refine grammar, spelling, or formatting – list each occurrence

(X) I acknowledge the use of ChatGPT and Grammarly to rephrase text incl. edit/refine grammar, spelling or formatting.

Eksempler på omformulering af tekst fundet i videnskabelige artikler/tekst jeg selv har omformuleret fra videnskabelige artikler (ChatGPT):

1. Kan du hjælpe med at omformulere denne sætning: IGF-1R is widely distributed throughout the rodent CNS, particularly in neuronal precursor cells, and shows significant expression during cerebellar maturation, midbrain development, olfactory bulb formation, and in the ventral hindbrain floor.
2. Kan du hjælpe med at omformulere denne sætning: If both isoforms of the INSR are co-expressed in cells, this can lead to the formation of homodimers, INSR-A or INSR-B.
3. Kan du hjælpe med at omformulere denne sætning: IGF-1R is a heterotetramer that structurally consists of two α-subunits and two β-subunits, similar structure to INSR.
4. Kan du hjælpe med at omformulere denne sætning: The brain is unique due to the BBB which forms tight junctions restricted insulin transport.

Eksempler på rettelser af grammatik (ChatGPT):

1. Er dette skrevet grammatisk korrekt: Besides promoting glucose uptake in adipocytes and skeletal muscle cells, insulin also triggers glycogenesis by promotes hepatocytes to store glucose as glycogen.
2. Er dette grammatisk korrekt: Currently, recent studies have found that BIR can also occur in the brain independently of diabetes.
3. Er dette skrevet grammatisk korrekt: Since insulin does not directly affect glucose uptake in the brain, the brain has in many years been considered as an insulin-insensitive organ.

Eksempler på rettelser af grammatik (Grammarly):

1. INSRa-A and INSRa-B were especially concentrated in the isolated capillary fractions rather than in total brain and brain fractions → vil rette til "primarily" i stedet for "especially"
2. The brain capillary depletion technique was used to separate brain capillaries from brain fractions. → vil slette "was used to separate", så der står "separated"
3. This suggests a potential association between metabolic changes in the brain and the development of AD → vil ændre det til: This suggests a potential association between brain metabolic changes and AD development.

10. Disclosure: Create presentations

☐ I acknowledge the use of XYZ, version, Month, Year (web URL) to explain what you used AI for. I entered the following prompts on Date, Month, Year:

Original prompt: "Paste the prompt"

Follow-up prompt: "Paste the prompt"

The output from these prompts was used to state what action was made using the output.

11. Disclosure: Communicate to laymen/non-specialists

☐ I acknowledge the use of XYZ, version, Month, Year (web URL) to explain what you used AI for. I entered the following prompts on Date, Month, Year:

Original prompt: "Paste the prompt"

Follow-up prompt: "Paste the prompt"

The output from these prompts was used to state what action was made using the output.

(X) ***I declare that the disclosure is complete and truthful.***

Student number: 20193684

Course: Master thesis

Date: 27/5-2025